Title

Retinoic acid-dependent loss of synaptic output from bipolar cells impairs visual information processing in inherited retinal degeneration.

Author List

Logan Ganzen[1†], Shubhash Chandra Yadav[1†], Mingxiao Wei[1], Hong Ma[1], Scott Nawy[1], Richard H Kramer[1]

1. University of California Berkeley, Department of Molecular and Cell Biology. Berkeley, CA, USA

† Authors contributed equally to this work.

Abstract

In retinitis pigmentosa (RP), rod and cone photoreceptors degenerate, depriving downstream neurons of light-sensitive input, leading to vision impairment or blindness. Although downstream neurons survive, some undergo morphological and physiological remodeling. Bipolar cells (BCs) link photoreceptors, which sense light, to retinal ganglion cells (RGCs), which send information to the brain. While photoreceptor loss disrupts input synapses to BCs, whether BC output synapses remodel is unknown. Here we report that synaptic output from BCs plummets in mouse models of RP owing to loss of voltage-gated Ca^{2+} channels. Remodeling reduces the dynamic range and the reliability of the BC output synapse to repeated optogenetic stimuli, eliminating RGC firing at high stimulus frequencies. However, the consequences of functional BC remodeling can be reversed by inhibiting the retinoic acid receptor (RAR). RAR inhibitors targeted to BCs present a new therapeutic opportunity for mitigating detrimental effects of remodeling on signals initiated by surviving photoreceptors or vision-restoring tools.

Introduction

Rod and cone photoreceptors degenerate in retinitis pigmentosa (RP) and age-related macular degeneration (AMD), depriving the visual system of light-evoked signals necessary for sight. The remaining retinal neurons can survive long after the rods and cones are gone. Critically, retinal ganglion cells (RGCs), the output neurons of the retina, remain connected to the brain [1,2]. This enables responses initiated by surviving photoreceptors to remain detectable late into disease progression [3]. The maintained connectivity of RGCs also provides a lifeline for restoring vision in profound blindness, either through regeneration of lost photoreceptors from stem cells, or introduction of light sensitivity in surviving retinal neurons with optoelectronic [4], optogenetic [5,6], or opto-pharmacological tools [7,8]. Whether direct or indirect, if a light stimulus can alter RGC firing appropriately, the response should be transmitted to the brain and result in visual perception.

Unfortunately, downstream neurons undergo remodeling that can corrupt the proper encoding of information and exacerbate vision loss [9]. Morphological remodeling can require months to develop in mice [10], while in contrast,

physiological remodeling begins almost immediately when photoreceptors die [11,12]. Many RGCs become hyperactive, spontaneously firing bursts of action potentials that obscure responses initiated by surviving photoreceptors. Patch clamp recordings show that the intrinsic electrical properties of RGCs are altered by photoreceptor degeneration [8] and transcriptional analysis shows altered expression of voltage-gated ion channels [13]. In addition, the plasma membrane of RGCs exhibits increased permeability to large dye molecules and azobenzene photoswitches, events attributed to increased expression of ATP-gated P2X receptors, which have a large pore [13].

How does photoreceptor death in the outer retina lead to physiological remodeling of RGCs in the inner retina? Retinoic acid (RA) is the key signal that triggers RGC hyperactivity and hyperpermeability [12]. Inhibitors of retinaldehyde dehydrogenase (RALDH), the enzyme that synthesizes RA, or RAR, the nuclear retinoic acid receptor, reduce hyperactivity and hyperpermeability. These agents also unmask responses of RGCs to dim light, sharpen responses of visual cortical neurons to patterns of illumination, and improve behavioral visual perception in vision-impaired mice with partial photoreceptor degeneration [9].

Bipolar cells (BCs) are located between photoreceptors and RGCs. During photoreceptor degeneration, input synapses exhibit morphological remodeling. BC dendrites, which normally invaginate the synaptic terminals of rods and cones, begin to retract [14], disconnecting the synapse. Synaptic transmission is also impaired by the loss or redistribution of dendritic mGluR6 receptors [15] and TRPM1 channels [16], which normally underlie the ON-BC response to the photoreceptor neurotransmitter glutamate. Despite these negative consequences, not all remodeling is counter-productive. The retina shows resilience by employing mechanisms that partially compensate for photoreceptor loss. Over time, new dendrites sprout from BCs and can re-establish synaptic connections in retinas with degenerated photoreceptors [17]. Experimental ablation of half of the rods in adults rebalances excitatory and inhibitory synaptic strength to BCs to restore proper RGC responses [18]. In young mice, partial ablation of cones leads to dendritic rewiring in certain BCs to restore the original number of input synapses [19].

In contrast, the question of whether the efficacy of the BC output synapse is changed by photoreceptor degeneration has remained unanswered. This is critical, as changes in BC output will alter the response properties of downstream RGCs, the only cell type that provides visual input to the brain. Here we evaluate the effects of photoreceptor degeneration on output synapses of two types of ON-BCs; rod bipolar cells (RBC), critical for scotopic vision and the most numerous BC type in mouse, and cone bipolar cell type-6 (CBC6), which plays a crucial role in all vision, from scotopic, to mesopic, to photopic. We find a dramatic reduction of voltage-gated Ca^{2+} current and neurotransmitter release from both RBCs and CBC6s, weakening transmission and decreasing the frequency response of the BC to RGC synapse. These effects can be reduced by inhibiting RA signaling, providing a potential therapeutic approach for abrogating the detrimental effects of BC remodeling in RP and AMD.

Results

63 **Voltage-gated calcium current in ON-BCs is reduced by photoreceptor degeneration.**

64 Voltage-gated calcium channels are critical for evoked neurotransmitter release at the BC output synapse [20]. To assess
65 whether photoreceptor degeneration alters activity of voltage-gated calcium channels, we measured membrane current
66 in whole-cell voltage-clamped BCs in retinal slices. We compared voltage-gated Ca^{2+} current in wildtype (WT) mice to
67 those in rd1 and rd10 mice, widely used animal models of RP. We focused on the Type-6 ON cone bipolar cell (CBC6),
68 which synapses directly onto RGCs, and rod bipolar cells (RBCs), which drive RGCs indirectly through a serial synapse on
69 the CBC output synaptic terminal (Figures 1a,d). Candidate BCs of each type were identified with cell-type selective gene
70 promoters that drive expression of a fluorescent protein reporter fused with channelrhodopsin-2 (ChR2-eYFP), namely
71 the CCK promoter for CBC6 cells and the PCP2 promoter for RBCs. The identity of individual BCs was confirmed by dye-
72 filling the cell to localize their terminals to specific sublamina in the inner plexiform layer (IPL) (Figure 1g).

73 We found that the voltage-gated Ca^{2+} current in CBC6 cells was 3-fold larger in WT mice than in rd1 or rd10 mice at
74 maximal activation (Figures 1b,c). Similarly, voltage-gated Ca^{2+} current in RBCs was 2-fold larger than in rd1 or rd10 mice
75 at maximal activation (Figures 1e,f). In both BC types, steady-state current vs. voltage curves showed reduced current
76 amplitude without any change in voltage-dependent activation (Figures 1c,f), consistent with a change in Ca^{2+} channel
77 number rather than a change in gating properties or channel type. We found that the L-type Ca^{2+} channel inhibitor
78 nimodipine eliminated the current in CBC6 cells (Figure S1) consistent with previous findings that L-type Ca^{2+} channels
79 predominate in BCs [21]. Photoreceptor degeneration occurs early in postnatal development in rd1 mice and later in
80 adulthood in rd10 mice, making certain aspects of morphological remodeling more severe in the rd1 strain [14]. Despite
81 this, the loss of Ca^{2+} current in CBC6 cells and RBCs was nearly identical in rd1 and rd10 mice.

82

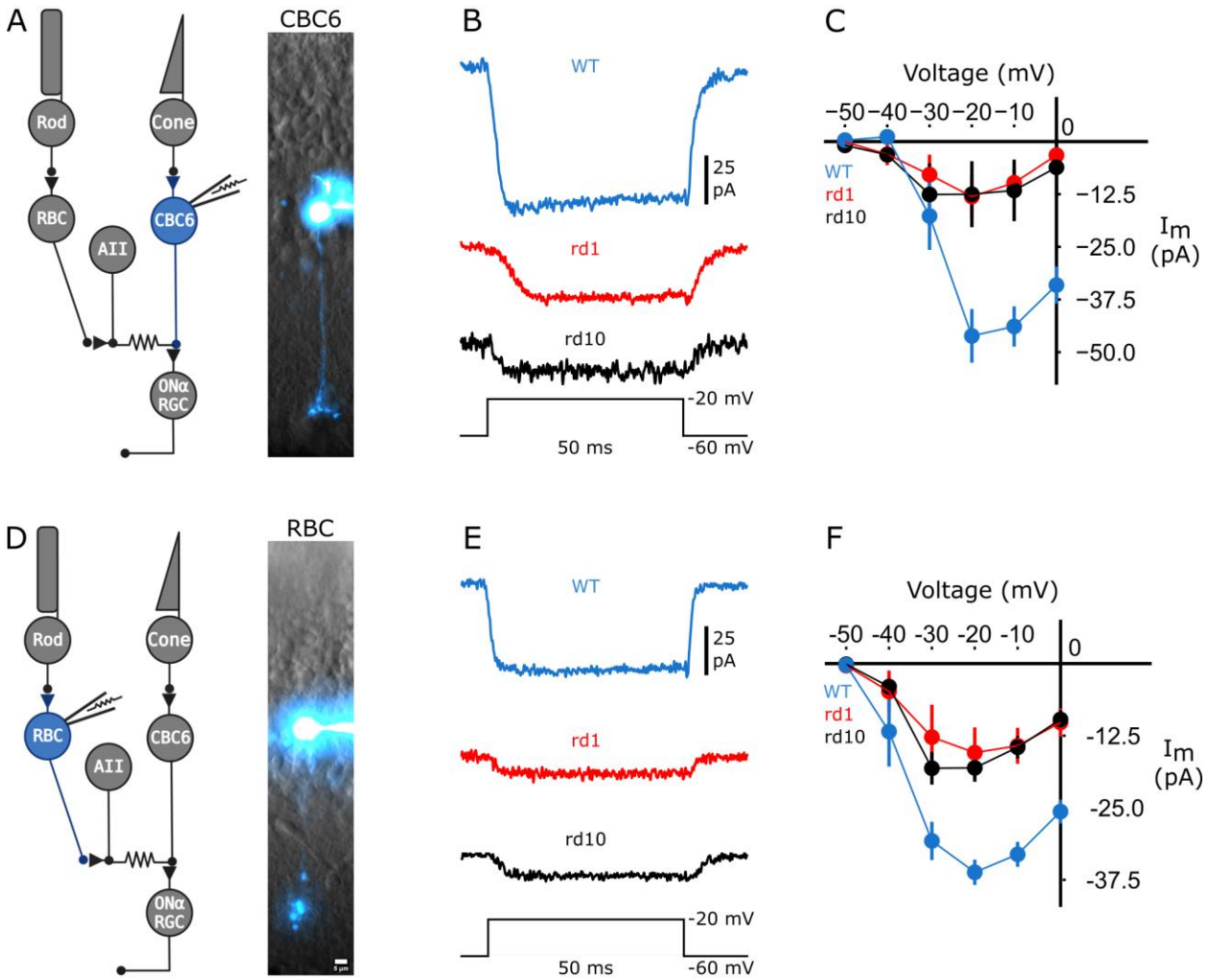

Figure 1. Voltage-gated calcium current of ON-BCs is reduced in photoreceptor degenerated retinas. A, B) Retinal circuit diagrams showing whole-cell patch-clamped CBC6 cells or RBCs with accompanying fluorescent dye fills (Alexa-Fluor 594) of a CBC6 cell or an RBC in a retinal slice. Scale bar = 5 µm. C, D) Inward calcium currents in BCs from WT, rd1, and rd10 retinas. Current was activated with a depolarizing voltage step (50 ms) from -60 mV to -20 mV. E, F) Steady-state current vs. voltage (I-V) curves, elicited with a series of 10 mV incrementing depolarizing steps from -60 to 0 mV (for CBC6 cells WT: N = 9; rd1: N = 5; rd10: N = 6; for RBCs, WT:N = 9; rd1:N = 6; rd10:N = 10). I-V curves from rd1 and rd10 BCs shows that the voltage-gated calcium current is lower than in WT BCs (Pairwise Wilcoxon Rank Sum Exact Test (PWT) with false discovery rate (FDR) correction (for CBC6: WT – rd1, p = 0.017; WT – rd10, p = 0.024. For RBC: WT – rd1, p= 0.006; WT – rd10, p-value = 0.001). Error bars indicate ± SEM.

Transmission at the BC output synapse is reduced by photoreceptor degeneration.

Neurotransmitter release is triggered by intracellular Ca^{2+}, hence the reduced Ca^{2+} current in BCs suggests that synaptic transmission will also be reduced. ON-BCs are ordinarily depolarized in the light, but in the absence of photoreceptors we can use optogenetics as an alternative to depolarize the cells and evoke synaptic release. We leveraged the cell-type selective expression of ChR2-eYFP to optogenetically depolarize either RBCs or CBC6s, in the WT, rd1, or rd10 background. To interrogate the BC output synapse in isolation, we blocked photoreceptor inputs onto BCs with the mGluR6 agonist L-AP4 and the kainate receptor antagonist ACET, which together eliminate light responses in all BCs [22]. We also blocked inhibitory synaptic inputs onto BCs with antagonists of ionotropic GABA and glycine receptors and electrical synapses with the gap junction uncoupler MFA.

We stimulated CBC6 cells with light flashes while we recorded evoked excitatory postsynaptic currents (EPSCs) from ON α-RGCs from whole-mount retinas (Figure 2a). Amongst the various BCs, this promoter enables transgene expression specifically in CBC6 cells, although sparse expression has been noted in non-BC cell types, including some ON type RGCs [23]. ON α-RGCs were identified by soma size and dendritic layer termination in the IPL, mapped after dye-filling. If a ChR2-eYFP expressing RGC was inadvertently targeted, it was removed from further consideration based on the exceedingly short optogenetic response delay and lack of susceptibility to the AMPAR antagonist DNQX (Figure S2).

Optogenetically evoked EPSCs in ON α-RGCs were smaller and slower in rd1 and rd10 than in WT retinas (Figure 2b). EPSCs were reduced across all stimulation strengths, including stimuli that saturated the synaptic response, consistent with diminished synaptic efficacy. EPSCs were ~40% smaller in rd1 and rd10 retinas with a saturating stimulus (Figures 2c,d). In addition, EPSC kinetics were slower in both rd1 and rd10, with a longer time-to-peak (Figure 2e). Patch clamp recordings of CBC6 cells expressing eYFP-ChR2 showed that the light-elicited current was nearly identical in WT, rd1, and rd10 retinas (Figure S3b), consistent with equal ChR2 expression. Furthermore, test flashes depolarized the cells equally (Figure S3). Hence the reduced EPSCs cannot be explained by reduced presynaptic depolarization in the degenerated retina, but rather by reduced synaptic efficacy. The output synapse also exhibited a striking loss of sensitivity in degenerated retina, most easily observed as a rightward shift in the plot of normalized responses vs. stimulus strength (Figure S4a). The stimulus required to evoke a half-maximal EPSC was nearly three times stronger in rd1 compared to WT retina (Figure S4c). Thus, the CBC6 output synapse exhibited a decrease in both peak response and sensitivity.

For examining the output synapse of RBCs, we expressed ChR2-EYFP under control of the Pcp2 promoter [24]. We optogenetically depolarized RBCs in retinal slices, recording EPSCs from their postsynaptic partner the AII amacrine cell. AII amacrine cells are electrically coupled to CBC6, indirectly driving RGC firing (Figure 2f). We recorded EPSCs in AII cells, which were identified after dye-filling by their distinctive cell body shape and dendritic terminations in the IPL. Synaptic output of RBCs onto AII cells was also reduced in rd1 and rd10 retinas as compared to WT (Figure 2g). Responses to saturating light at the RBC synapse were reduced by ~75% in rd1 retinas and ~65% in rd10 retinas as compared to WT with a saturating stimulus (Figures 2h,i). There was also a loss of synaptic sensitivity, although less striking than the loss

127 at the CBC6 output synapse (Figures S4b,d). RBCs ordinarily exhibit highly synchronous release, resulting in rapid and
128 transient postsynaptic responses [25], but the responses were slower to rise and more prolonged in degenerated retina,
129 implying that degeneration promotes more asynchronous transmitter release from RBCs. The time-to-peak of evoked
130 EPSCs was 2- or 3-fold longer, for rd10 and rd1 retinas as compared to WT (Figure 2e,j). In summary, the output
131 synapses of both CBC6 cells and RBCs show dramatically reduced synaptic efficacy, consistent with reduced Ca^{2+}-
132 dependent neurotransmitter release.

133

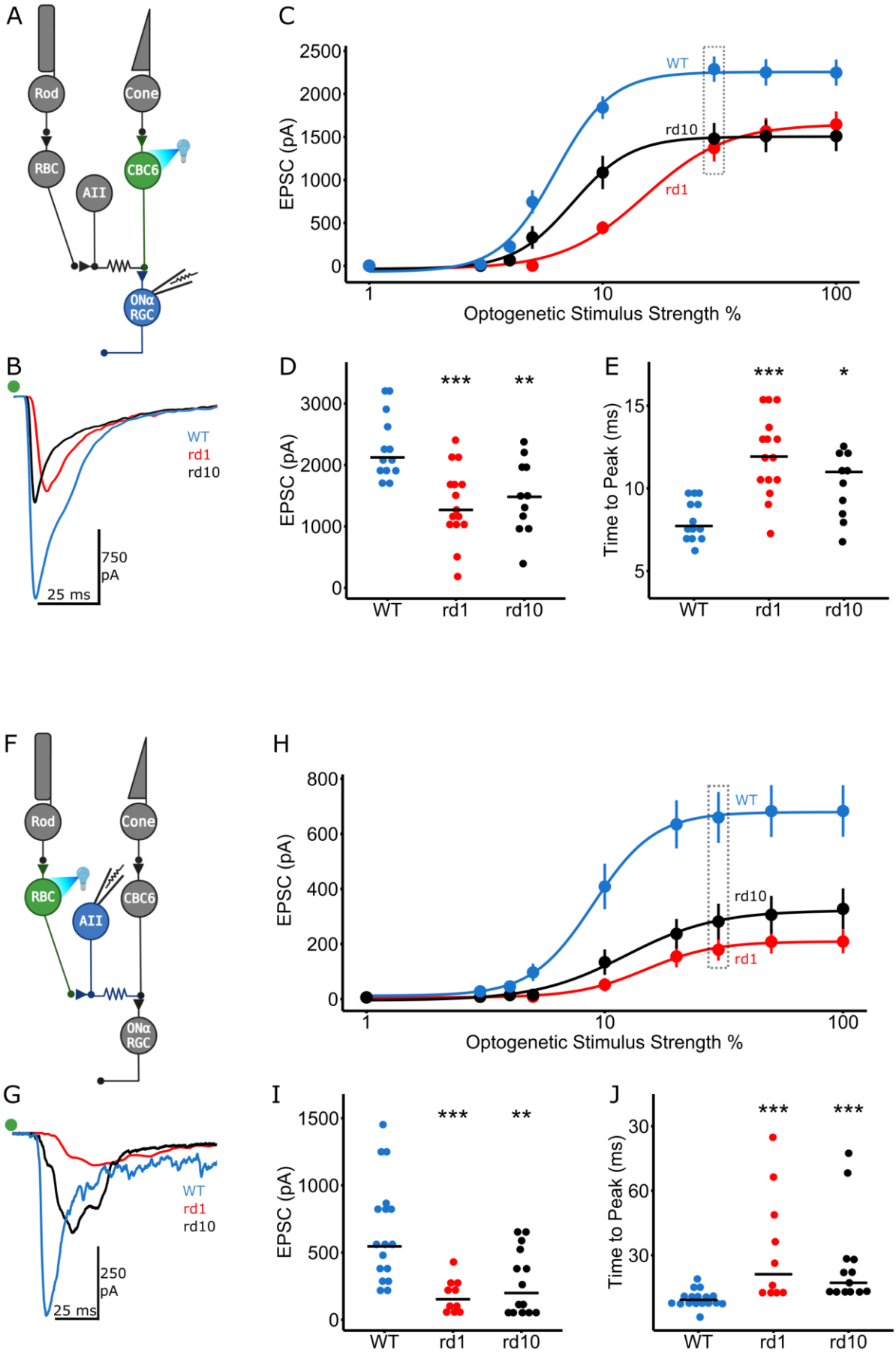
A
Rod
Cone
RBC
AII
CBC6
ONα RGC
B
WT
rd1
rd10
750 pA
25 ms
C
EPSC (pA)
Optogenetic Stimulus Strength %
WT
rd10
rd1
D
EPSC (pA)
***
**
WT
rd1
rd10
E
Time to Peak (ms)
***
*
WT
rd1
rd10
F
Rod
Cone
RBC
AII
CBC6
ONα RGC
G
WT
rd1
rd10
250 pA
25 ms
H
EPSC (pA)
Optogenetic Stimulus Strength %
WT
rd10
rd1
I
EPSC (pA)
***
**
WT
rd1
rd10
J
Time to Peak (ms)
***
***
WT
rd1
rd10

134

135

136 **Figure 2. Synaptic output from ON-BCs is reduced in photoreceptor degenerated retinas.** A,F) Retinal circuit diagrams
137 showing optogenetically stimulated CBC6 cells or RBCs. EPSCs were recorded from a postsynaptic ON α-RGC or AII
138 amacrine cell, respectively. B,G) EPSCs in CBC6 cells (B) and RBCs (G). Note the reduced EPSCs in rd1 and rd10 retinas
139 compared to WT. The green dot represents the light flash. C,H) At all effective optogenetic stimulus strengths, EPSCs
140 from CBC6 cells (C) and RBCs (H) were smaller in rd1 and rd10 than in WT (For CBC6 cells: rd1 vs. WT: $p<0.001$; rd10 vs.
141 WT: $p = 0.009$; rd1:N=15, rd10:N=11, WT:N=13. For RBCs: rd1 vs. WT: $p<0.001$; rd10 vs. WT: $p<0.001$; WT:N=17,
142 rd1:N=10, rd10:N=14). D,I) EPSCs elicited by a saturating stimulus (dashed box in panels C and H) were smaller in rd1
143 and rd10 than in WT (For CBC6 cells: rd1= 1.27 nA, rd10 = 1.48 nA, WT = 2.12 nA; rd1 vs. WT: $p <0.001$; rd10 vs. WT: $p =$
144 0.008; for RBCs: rd1 = 152 pA, rd10 = 198 pA, WT = 546 pA; rd1 vs. WT: $p <0.001$; rd10 vs. WT: $p = 0.007$). E,J)Rise time
145 of EPSCs is slower in rd1 and rd10 than in WT retinas for both the CBC6 output synapse (rd1 = 11.92 ms, rd10 = 10.99
146 ms, WT = 7.72 ms; rd1 vs. WT, $p <0.001$; rd10 vs. WT, $p = 0.011$) and the RBC output synapse (rd1 = 21.17 ms, rd10 =
147 19.19 ms, WT = 9.24 ms; rd1 vs. WT, $p <0.001$; rd10 vs. WT, $p <0.001$). For panels D, E, I and J, each data point represents
148 peak EPSC from an individual recording; horizontal lines represent median EPSC values; error bars indicate ± SEM. All
149 statistical comparisons were made with PWT with FDR correction.

150

151 **Morphological analysis shows that the number of output synapses from CBC6 cells is unaltered by photoreceptor**
152 **degeneration.**

153 Reduced synaptic transmission could either be caused by a decrease in the number of synaptic contacts between pre-
154 and postsynaptic neurons or caused by a decrease in the synaptic efficacy with no change in synapse number. To
155 discriminate between these possibilities, we used immunohistochemistry and fluorescence microscopy to quantify the
156 density of CBC6 synaptic contacts onto ON α-RGC dendrites in the IPL. We used antibodies against secretagogin to
157 visualize the axon terminals of CBC6 cells. Secretagogin labels CBC types 2,3,4, 5, 6 in the mouse retina. CBC2-4 types are
158 OFF-BCs that terminate in distant off sublamina, CBC5 stratify in IPL 3, so CBC6 terminals can be identified
159 unambiguously in the IPL 4 [26]. CBC6 cells constitute more than 70% of bipolar synaptic inputs to ON α-RGC [27] while other
160 ON-CBC types sharing stratification with ON α-RGCs lack secretagogin expression [28]. BC terminals possess synaptic
161 ribbons, which we labeled with a fluorescent antibody against ribeye, the main structural protein in the ribbon. Finally,
162 we visualized the dendritic tree of an individual ON α-RGC by dye-filling the cell (Figure 3a).

163 Confocal microscope images from the IPL show CBC6 terminals overlapping with ON α-RGC dendrites (Figure 3b). To
164 restrict our analysis to functional synapses, we examined the overlap between ON α-RGC dendrites and ribeye-labeled
165 puncta (CtBP2) within CBC6 terminals (Figures 3c-e). We found that the number of putative synapses onto the ON α-RGC
166 was the same in WT and rd1 retinas (Figure 3f). The number of synapses per unit area of the ON α-RGC was also the
167 same (Figure 3g). By focusing through the depth of the IPL, we reconstructed the terminal tree of an individual CBC6 cell,
168 which is displayed as a flattened 2D projection (Figure 3h). Imaging ribeye puncta overlapping with the terminal tree
169 revealed the total number of presumptive ribbon synapses formed by that CBC6 cell (Figure 3i,j). Using this approach,
170 we found no difference in the number of CBC6 cell output synapses between WT and rd1 retinas (Figure 3k).
171 Additionally, there was no difference in the density of ribbons per axon terminal (Figure 3l). We conclude that there is
172 no difference in the number of presumptive CBC6 synapses between WT and rd1 retina.

173

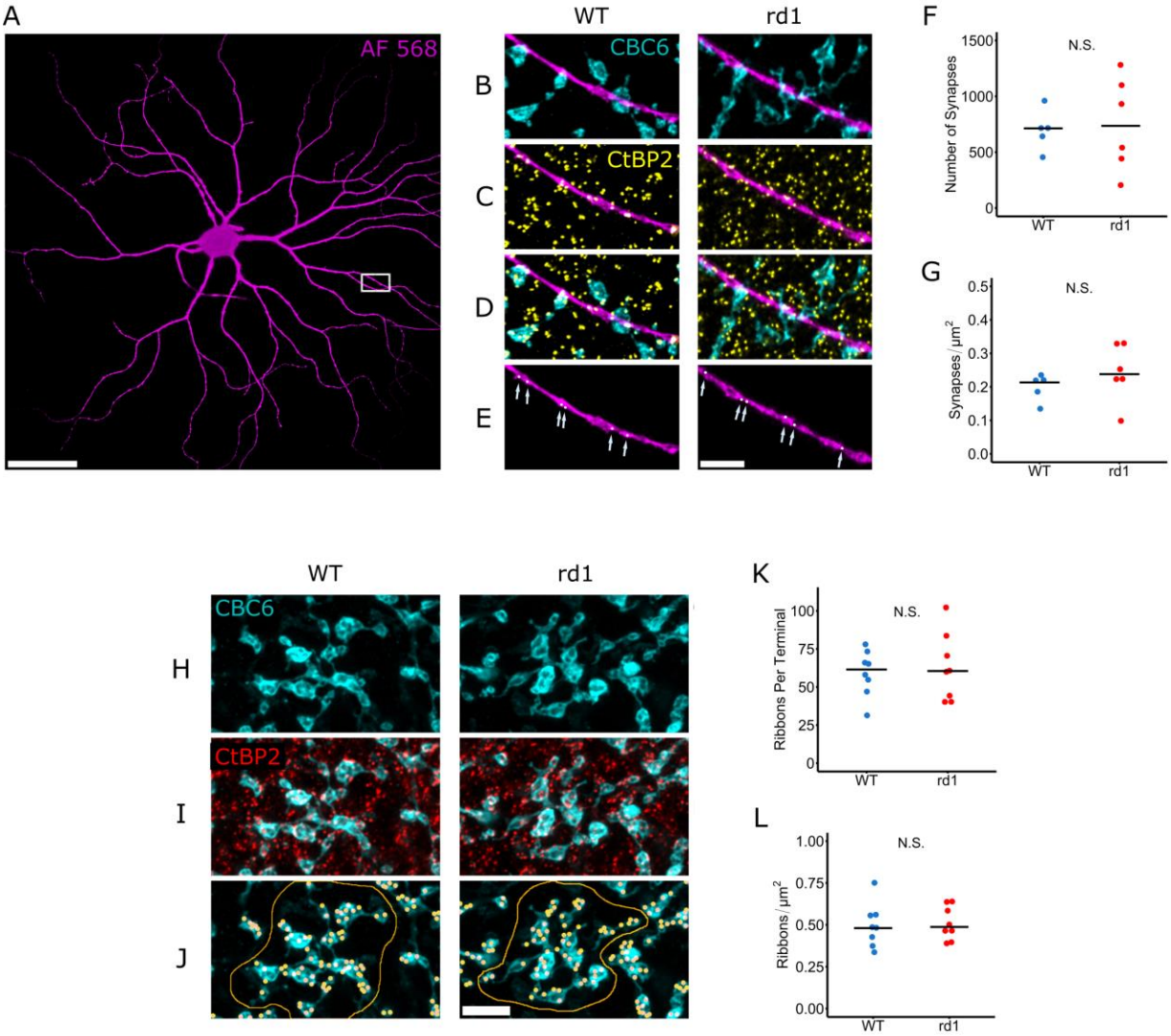

Figure 3. CBC6 cell output synapse morphology is unaltered by photoreceptor degeneration. A) Soma and dendrites of an ON α-RGC, labeled by intracellular injection with Alexa Fluor 568. Image is a 3-D projection from a stack of confocal optical sections. B-E) Magnified view of one ON α-RGC dendrite (magenta), overlapping with CBC6 axon terminals (B), labeled with anti-secretagogin (cyan), C) overlapping with synaptic ribbons, labeled with anti-CtBP2 (yellow), D) overlapping with synaptic ribbons exclusively in CBC6 terminals, identified by co-labeling with anti-secretagogin and anti-CtBP2. E) Arrows point to sites of co-localization between the dendrite, CBC6 axon terminals, and CtBP2, i.e., presumptive ribbon synapses between CBC6 cells and the ON α-RGC. F, G) Quantification of the total number of CBC6 ribbon synapses across all optical sections of the dendritic tree of an ON α-RGC (F) and the density of CBC6 ribbon synapses per unit area of the ON α-RGC. (G). There is no significant difference in the number (WT vs. rd1: $p = 1$) or density of ribbon synapses (WT vs. rd1: $p = 0.33$) in rd1 vs. WT retinas. WT: N=5, rd1: N=6. H)2D projection of the 3D structure of axon terminals of CBC6 cells in WT and rd1 retinas. I) CBC6 axon terminal overlapping with CtBP2. J) CBC6 axon terminals with yellow dots denoting thresholded points of overlap with CtBP2. The red outline indicates the axon terminal tree of one individual CBC6 cell. K, L) Quantification of the number of CtBP2 sites per CBC6 axon terminal tree (K) and the density of CtBP2 sites per CBC6 axon terminal tree (L). There is no significant difference in the number (WT vs. rd1: $p = 0.33$) or density (WT vs. rd1: $p = 1$) of ribbon synapses made by an individual CBC cell onto an ON α-RGCs in rd1 vs. WT retinas. WT: N=8, rd1: N=8. Scale bars: A (50 µm); B-E, H-J (5 µm). All statistical comparisons were made with PWT with FDR correction.

192 **Electrically evoked glutamate release from BC terminals is reduced by photoreceptor degeneration.**

193 The described results suggest that decreased synaptic efficacy from BC to postsynaptic cells in the photoreceptor-
194 degenerated retina is caused by decreased release of the neurotransmitter glutamate. To directly confirm reduced
195 glutamate release, we used the genetically encoded glutamate indicator iGluSnFR, delivered to RGCs with an AAV vector
196 that transduces diverse types of RGCs indiscriminately. After allowing 2-3 weeks for viral transduction and gene
197 expression, we isolated and mounted the retina in a chamber that enables simultaneous trans-retinal electrical
198 stimulation and 2-photon imaging (Figure 4a). By focusing on different depths through the inner retina, we obtained
199 virtual cross-sections of the IPL, which showed similar baseline levels of iGluSnFR expression in WT and rd1 retinas
200 (Figure 4b). We placed electrodes across the thickness of the retina to enable electrical stimulation of all cells. To
201 examine neurotransmitter release from BCs output synapse in isolation, we pharmacologically blocked all input synapses
202 to BCs. Under these conditions, we found that a brief electrical stimulus (10 ms) evoked a transient increase in iGluSnFR
203 fluorescence in the ON-layer of the IPL that was smaller in rd1 than in WT (Figure 4c). The peak change in fluorescence
204 over background ($\Delta F/F_0$) was 75% smaller in rd1 than in WT (Figures 4d,e). We were concerned that retinas lacking
205 photoreceptors might have altered tissue resistance, which could impact the effectiveness of electrical stimulation of
206 BCs. To address this point, we varied electrical stimulus strength to generate a range of responses, from no detectable
207 iGluSnFR signal to a saturating signal (Figure 5f). We found that while the magnitude of the response to all stimuli
208 (including the saturating stimulus) was lower in rd1, the sensitivity was the same, indicating that the reduced response
209 could not be attributed to less effective electrical stimulation (Figures 4f). Furthermore, peak iGluSnFR $\Delta F/F$ in response
210 to application of 10 mM glutamate was no different in WT and rd1 retinas, ruling out the possibility of impaired iGluSnFR
211 expression in rd1 retina (Figure 4g). Taken together, these results suggest that reduced synaptic efficacy in degenerated
212 retina is caused by reduced evoked glutamate release from ON-BCs.

213

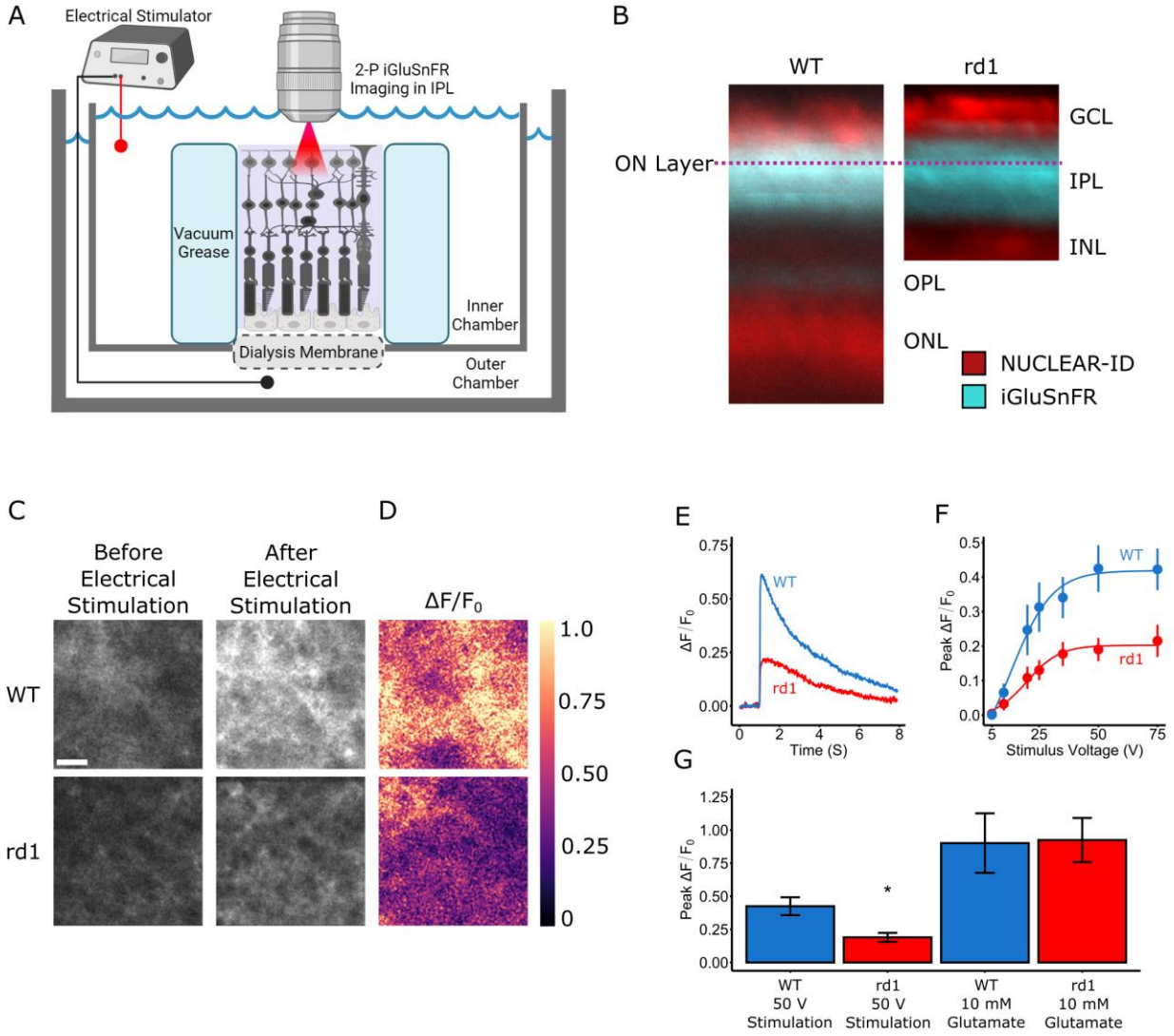

Figure 4. Synaptic release of glutamate from ON-BCs is reduced in retinas with photoreceptor degeneration. A) Apparatus for simultaneous trans-retinal electrical stimulation and 2-photon imaging of glutamate, the BC neurotransmitter. B) Virtual cross-sections (z-stacks) of retinas imaged with 2-photon microscopy. The genetically encoded fluorescent glutamate indicator iGluSnFR (cyan) was virally expressed throughout the IPL of WT) and rd1 retinas. The dashed line represents the ON Layer imaging plane, 10 µm into the IPL from the GCL border. Cell body layers were counterstained with a DNA-binding dye (NUCLEAR-ID, red). C) An optical section within the ON layer of the IPL before and 15 ms after stimulation, consisting of a 50 V, 2.5 ms shock in WT and rd1. D) The change in iGluSnFr fluorescence over background (ΔF/F), proportional to the change in glutamate concentration. Note that the fluorescence change upon stimulation is smaller in rd1 than in WT. E) Time course of the fluorescence change elicited by a single 2.5 ms, 50 V shock in a WT and rd1 retina. F) Peak iGluSnFR ΔF/F in response to varying shock strength. G) Peak iGluSnFR ΔF/F in response to a saturating 50 V, 2.5 ms shock is lower in rd1 than in WT ($p = 0.02$, $N = 7$ retinas). Peak iGluSnFR ΔF/F in response to application of 10 mM glutamate is no different between WT and rd1 retinas ($p = 0.71$, $N = 7$ retinas). Barplots indicate median value; error bars indicate ± SEM. Scale bar: 5 µm. All statistical comparisons were made with PWT with FDR correction.

230 **Retinoic acid mediates physiological remodeling of BCs**

231 RA triggers physiological remodeling of RGCs in the degenerated retina. To explore whether RA also underlies
232 physiological remodeling of BCs we treated mice with BMS 493, an inverse agonist of the RA receptor, RAR [29]. Because
233 the effects of RA are mediated by changes in gene expression, which may require days to take effect, we injected BMS
234 493 into the vitreous 5-7 days before retinal recording. First, we measured voltage-gated Ca^{2+} current from BCs in retinal
235 slices. BMS 493 increased the current by ~3-fold in both CBC6 cells from rd1 mice and in RBCs from rd10 mice at
236 maximal activation while causing no change in voltage-dependent activation, as shown in steady-state I-V curves (Figure
237 5a,b). In contrast, BMS 493 caused no change in Ca^{2+} current in CBC6 cells from WT mice (Figures S5). Next, we
238 examined the effect of inhibiting RA signaling on the synaptic output of BCs in degenerated retinas. BMS 493 increased
239 optogenetically-elicited synaptic transmission from CBC6 cells by ~35% in rd1 retina and ~45% in rd10 retina with a
240 saturating stimulus (Figure 5c), nearly completely reversing the deficit caused by photoreceptor degeneration (see
241 Figure 2c). BMS 493 also increased synaptic transmission from RBCs, by 30% in rd1 retina and 50% in rd10 with a
242 saturating stimulus (Figure 5d), reducing the photoreceptor degeneration deficit (see Figure 2c).

243 Inhibiting RA signaling also had dramatic effects on short-term synaptic plasticity, which is altered in photoreceptor
244 degenerated retina. In WT retinas, the BC output synapse exhibits profound paired-pulse depression, consistent with the
245 large Ca^{2+} current eliciting so much neurotransmitter release that the readily-releasable pool of synaptic vesicles is
246 depleted by the first stimulus, leaving little to be released by the second stimulus (Figure 5e,f) [30,31]. In rd1 or rd10
247 retinas, there is little paired-pulse depression, consistent with smaller Ca^{2+} current evoking less release, preserving the
248 readily releasable vesicle pool. BMS 493 caused more synaptic depression in and vesicle depletion in rd1 retinas similar
249 to WT. Injecting all-trans RA (ATRA), a relatively stable isomer of RA, into WT eyes reduced the amplitude of
250 optogenetically-evoked EPSCs and reduced paired-pulse depression, suggesting that RA signaling is sufficient to trigger
251 changes in the BC output synapse. Taken together, these findings implicate RA as the key signal that induces
252 physiological modeling of BCs.

253

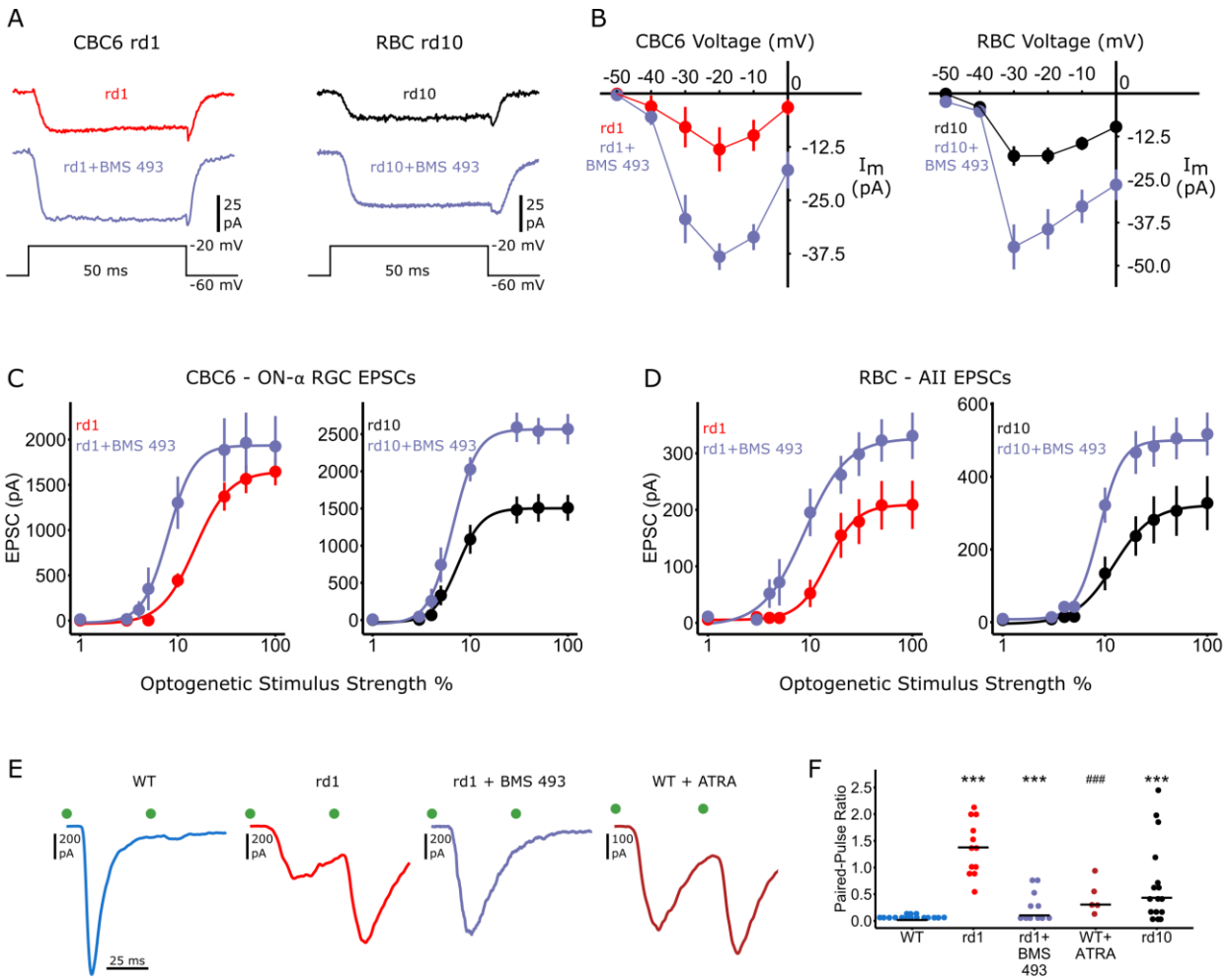

Figure 5. RA signaling is necessary and sufficient for physiological remodeling of BCs. A) Inward calcium currents in BCs treated with BMS 493 from rd1 CBC6 or rd10 RBCs. Current was activated with a depolarizing voltage step (50 ms) from -60 mV to -20 mV. B) Steady-state current vs. voltage (I-V) curves, elicited with a series of 10 mV incrementing depolarizing steps from -60 mV. I-V curves show that the BMS 493 significantly rescues voltage-gated calcium current in both CBC6 cells in rd1 retina ($p < 0.001$) and RBCs in the rd10 retina ($p < 0.001$). CBC6 cells: rd1, N = 5; rd1 + BMS 493, N = 5. RBCs: rd10, N = 10, rd10 + BMS 493, N = 7. C) EPSC magnitude vs. optogenetic stimulus strength. BMS 493 increased EPSC magnitude in ON α-RGCs in rd1 ($p=0.006$) and rd10 retinas ($p<0.001$). RGCs: rd1, N = 15; rd1 + BMS 493, N = 11; rd10 N = 11; rd10 + BMS 493, N = 8. D) BMS 493 also increased EPSC magnitude in AII amacrine cells in rd1 ($p=0.001$) and rd10 retinas ($p<0.001$). AII cells, rd1: N=10, rd1 + BMS 493: N=9, rd10: N=14, rd10 + BMS 493: N=12. E) EPSCs from ON α-RGCs in response to paired pulse flashes given with a 50 ms interval. Green dots indicate light flash. WT shows complete paired-pulse depression and rd1 shows no paired-pulse depression. Note that BMS 493 induces paired-pulse depression in rd1 and ATRA eliminates paired-pulse depression in WT. F) Quantification of the paired pulse ratio (EPSC 2 / EPSC 1). Compared to WT, paired EPSCs exhibited less synaptic depression in rd1 ($p<0.001$), rd10 ($p=0.004$), and ATRA-treated WT retinas ($p<0.001$) denoted with ***. BMS 493 treatment increased synaptic depression in rd1 retinas ($p<0.001$) denoted with ###. WT: N=16, rd1: N=13, rd10: N=16, rd1 + BMS 493: N=11, WT + ATRA: N=5. Horizontal lines indicate median values: WT=0.02, rd1=1.38, rd10=0.43, rd1 + BMS 493=0.10, WT + ATRA=0.30 . Error bars indicate ± SEM. All statistical comparisons were made with PWT with FDR correction.

273 **Physiological remodeling of BCs alters spatiotemporal information processing.**

274 In the WT retina, sensory information from an array of photoreceptors signals through a series of retinal neurons,
275 ultimately converging onto an RGC to produce a classical receptive field. In a photoreceptor-degenerated retina with the
276 responses of a particular type of BC under optogenetic control, each RGC receives a projective field, reflecting the
277 convergence of information from that specific BC cell type. Here we compare rd1 and WT retinas to ask whether
278 photoreceptor degeneration alters the CBC6 to ON α-RGC projective field. We optogenetically stimulated small clusters
279 of CBC6 cells with 50 µm spots of light to yield a spatial map of BCs projecting onto an individual ON α-RGC (Figures 6a-
280 c). We found that the spatial map in rd1 retinas is nearly identical to the map in WT retina, but scaled down linearly
281 (Figures 6d,e), presumably owing to decreased synaptic transmission. This finding is consistent with previous work
282 showing little change in cone-mediated RGC receptive field size following rod degeneration, in a different mouse model
283 of RP [32].

284 We next compared the temporal properties of the CBC6 to ON α-RGC network in WT and photoreceptor degenerated
285 retinas. We optogenetically stimulated populations of CBC6 cells at different rates and recorded either EPSCs in whole-
286 cell patch recordings or spiking in cell-attached patch recordings from individual RGCs (Figure 7a). In the WT retina, a
287 low frequency train of stimuli (0.25 Hz) evoked a non-decrementing train of EPSCs (Figures 7b,c). Even with higher
288 frequency stimulation (up to 7.5 Hz), EPSCs followed reliably, although their amplitudes declined during the train
289 (Figures 7b-e). In rd1 and rd10 retinas, EPSCs were non-decrementing at low frequency (0.25 Hz), but their amplitudes
290 declined rapidly at higher frequencies, with EPSCs failing completely by the end of the 7.5 Hz stimulation train.
291 Comparing across all stimulation rates, the frequency at which EPSCs declined by 90% (-10 dB) at steady state was 5.25
292 Hz for WT , 0.68 Hz for rd1, and 2.47 Hz for rd10. (Figure 7f).

293 Decrementing synaptic efficacy would be expected to adversely impact action potential reliability in RGCs. To test this,
294 we made cell-attached patch-clamp recordings to non-invasively monitor spike activity from ON α-RGCs. In the WT
295 retina, RGC firing followed optogenetic BC stimulation reliably up to 7.5 Hz (Figure 7g), consistent with temporal tuning
296 of normal light responses in ON α-RGCs in WT retinas [22]. In the rd1 and rd10 retina, firing failed to follow even at 2.5 Hz
297 stimulation frequency. We compiled firing reliability data over a wide range of stimulus frequencies and train durations.
298 RGCs failed to follow BC stimulation at a low frequency in rd10 and an even lower frequency in rd1 (Figure 7h). The
299 decline of reliability in the CBC6 to ON α-RGC network can be attributed entirely to changes in the BCs, as there is no
300 difference in the response of ON α-RGC to firing induced by direct current injection in WT and degenerated retinas
301 (Figure S6). These findings illustrate the severe deficit that BC physiological remodeling imposes on information transfer
302 to RGCs in the degenerated retina.

303 Equivalent experiments on RBC output synapse showed an even more extreme frequency-dependent decline in
304 photoreceptor degenerated retina (Figures 8a,b). Even at 0.25 Hz, EPSCs from rd1 and rd10 retinas began decrementing
305 while WT did not (Figure 8b,c). Higher stimulation frequency led to the near complete loss of EPSCS in rd1 and rd10 at

306 steady state (Figure 8b,d,e). Comparing all stimulation rates, the frequency at which EPSCs declined by 90% (-10 dB) at
307 steady state was 5.14 Hz for WT, 0.69 Hz for rd1, and 1.34 Hz for rd10. (Figure 8f). Since the vast majority of ON BC types
308 receive direct or indirect input from RBCs, the decrementing responses in photoreceptor degenerated retinas is
309 expected to adversely impact a wide variety of ON-RGCs beyond just the ON α-RGC subtype.

310

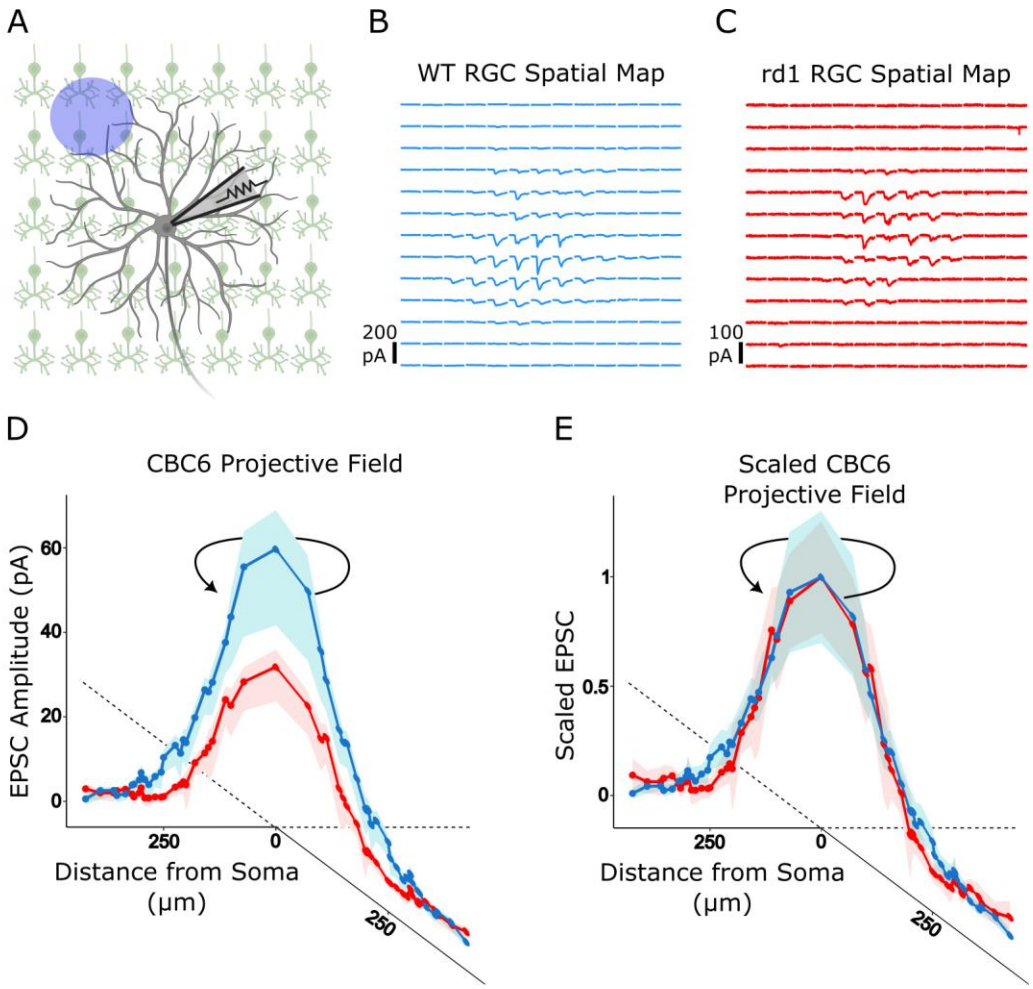

Figure 6. The spatial map of the BC to RGC network is preserved in photoreceptor degenerated retina but scaled down linearly. A) Schematic diagram of the experiment. To map the projective field corresponding to many CBC6 cells converging onto a single ON α-RGC, we used 50 µm non-overlapping spots of light to optogenetically stimulate clusters of BCs, covering the entire dendritic tree of the ON α-RGCs. B-C) Example spatial projective field map from a WT (B) and rd1 (C) retina. Detectable EPSCs were elicited over ~200 μm^2 of the 650 μm^2 mapped area. D) Group data from ON α-RGCs (N=9 each), with the projective field represented as mean EPSC vs. distance from the cell soma. Data from all directions from the cell center were averaged and are shown duplicated for clarity. Note that EPSCs were smaller in rd1 than WT (p=0.012), but there was no difference in spatial weighting of the linearly scaled projection field (p=0.47). Variability ribbons indicate 95% confidence intervals. All statistical comparisons were made with PWT with FDR correction.

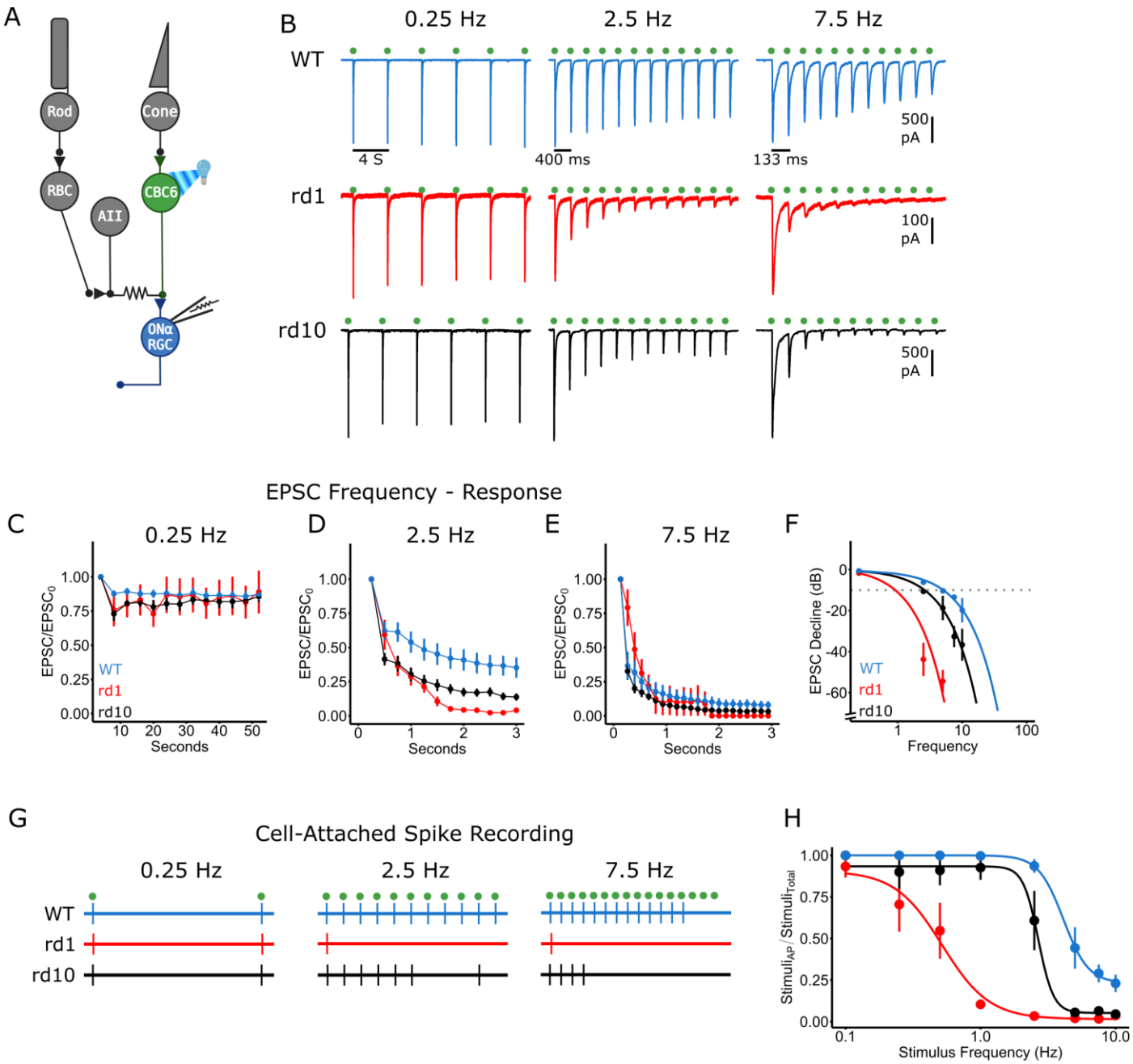

Figure 7. Photoreceptor degeneration reduces the frequency response in the cone pathway. A) CBC6 cells were optogenetically stimulated at different rates while EPSCs were recorded in an ON α-RGC. B) EPSCs elicited by stimuli repeated at 0.25 Hz, 2.5 Hz, and 7.5 Hz. Green dots indicate the time of light flash. C – E) EPSCs in rd1 and rd10 retinas diminish faster with increasing stimulation frequency. F) EPSC decline expressed in dB ($10Log\frac{EPSC_{Final}}{EPSC_{Initial}}$) for each stimulation frequency. The continuous line is the fit with a linear function. (WT: N=7, $y = -0.143 - 1.93x$, R^2= 1.00; rd1: N = 9, $y = 1.42 - 12.5x$, R^2= 0.99,; rd10: N=10 $y = 0.272 - 3.93x$, R^2= 0.95). The dotted line is $y = -10\ dB$. EPSCs for rd1 at 7.5 and 10 Hz become immeasurably small at steady state. G) Raster of cell-attached spike recordings from stimulation at 0.25 Hz, 2.5 Hz, and 7.5 Hz. Green dots indicate light flash. H) The ratio of stimuli that produced an action potential to the total number of stimuli per frequency. Compared to WT, rd1 and rd10 ON α-RGCs successfully encoded fewer stimuli as stimulation frequency increased. WT: N=6, rd1, N=6, rd10, N = 5 cells.(rd1: p<0.001, rd10: p=0.034. PWT with FDR correction).

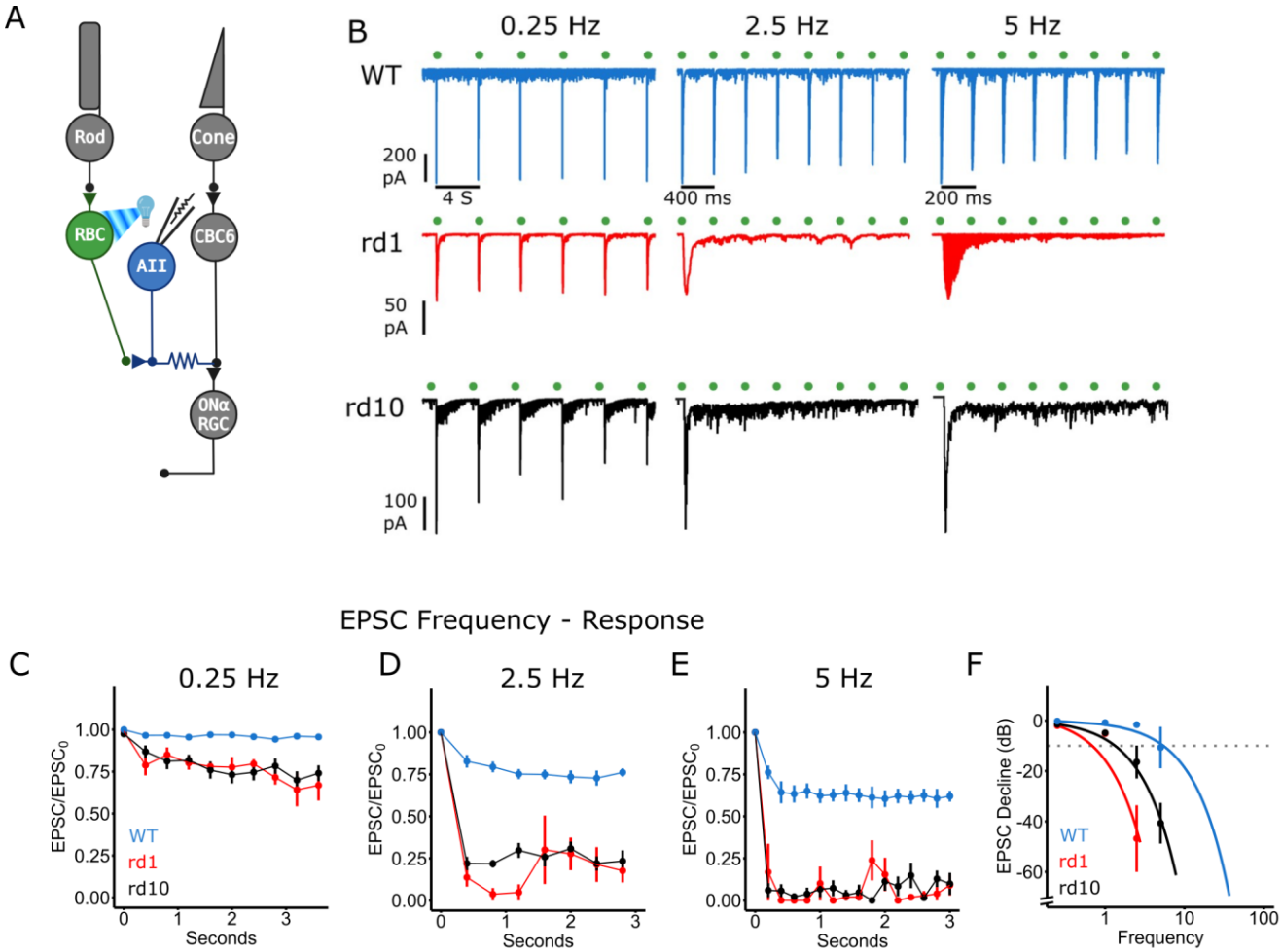

Figure 8. Photoreceptor degeneration reduces the frequency response in the rod pathway. A) RBCs cells were optogenetically stimulated at different rates while EPSCs were recorded in an AII amacrine cell. B) EPSCs elicited by stimuli repeated at 0.25 Hz, 2.5 Hz, and 5 Hz. Green dots indicate the time of light flash. C – E) EPSCs in rd1 and rd10 retinas diminish faster with increasing stimulation frequency. F) EPSC decline expressed in dB ($10Log\frac{EPSC_{Final}}{EPSC_{Initial}}$) for each stimulation frequency. The continuous line is the fit with a linear function. (WT: N=6, $y = -0.28 - 1.89x$, R^2= 0.90; rd1: N=5, $y = 2.63 - 18.4x$, R^2= 0.99,; rd10: N=11, $y = 0.579 - 7.91x$, R^2= 0.94). The dotted line is $y = -10\ dB$. EPSCs for rd1 at 5 Hz become immeasurably small at steady state.

345 **Discussion**

346 This paper reports the surprising finding that photoreceptor degeneration leads to dramatic functional weakening of the
347 output synapses of ON-BCs. RBCs, the most numerous type of BC in the rod-dominant mouse retina, and CBC6 cells,
348 which receive information from both rod and cone pathways, are both affected. The net effect of these changes in BCs
349 is to reduce the amplitude and narrow the frequency response of light onset signals sent to RGCs and onward to the
350 brain. Our imaging results with iGluSnFr suggests that glutamate release from OFF-BCs might also be reduced in the
351 degenerated retina, which might also reduce signals at light offset. New cell-type selective promoters for particular OFF-
352 BCs could help address this point.

353 Previous experiments on a rat model of RP showed that ON-RGCs exhibit reduced spontaneous firing, paralleling the loss
354 of the RGC light response [33]. The most obvious explanation for the decline in spontaneous and evoked ON-RGC activity
355 is that the diminishing number of photoreceptors drives a declining amount of excitatory synaptic input. However, the
356 possibility that changes intrinsic to ON-BCs also contributed to changes in ON-RGC activity remained unexplored. Our
357 discovery that the output synapse of ON-BCs is dramatically weakened adds an important new mechanism that may
358 contribute to changes in ON-RGC activity across species, not only corrupting retinal signal processing, but also
359 contributing to the pathophysiology of vision loss.

360 Another consequence of photoreceptor loss is the emergence of membrane potential oscillations in the inner retina,
361 ultimately resulting in spontaneous burst firing in RGCs [34]. The oscillation is initiated in the electrically coupled network
362 of AII amacrine cells [35], but it remains to be determined if RA-mediated events are involved.

363 **Mechanism of physiological remodeling**

364 Our findings suggest that RA is necessary and sufficient for physiological remodeling of the ON-BC output synapse.
365 Adding exogenous ATRA mimics changes in synaptic release that are characteristic of degenerated retinas (Fig. 4e).
366 Inhibiting RAR with BMS 493 reverses changes in synaptic release and restores voltage-gated Ca^{2+} current to near WT
367 levels (Fig. 4). Our previous studies utilizing an RA-induced reporter demonstrated elevated RA-induced gene expression
368 in degenerated retina [12].

369 It remains unclear where the excessive RA is produced. RA has been implicated in physiological remodeling not only in
370 the output synapses of BCs but also in RGCs [12]. Moreover, RA is critical for morphological remodeling of BC dendrites, at
371 their input synapses [17]. The fact that multiple cell types are affected in a degenerated retina suggests that RA might act
372 in a paracrine fashion, produced by one cell type (perhaps RPE cells), and diffusing throughout the retina to trigger
373 remodeling in many cell types. Immunocytochemistry and enzyme assays show that the retina, choroid, and RPE all
374 express isoforms of RALDH, the enzyme that synthesizes RA [36]. In the RPE, RALDH normally converts all-trans
375 retinaldehyde released from photobleached rhodopsin into RA [37]. The loss of photoreceptors might increase the
376 concentration of retinaldehyde, leading to increased production of RA by the RPE. In this scenario, RA would be an

377 intercellular signal, diffusing from the outer to the inner retina to exert its actions. Alternatively, it is possible that RA is
378 synthesized within particular retinal neurons and serves as an intracellular messenger. In neurons in the hippocampus,
379 local production of RA in dendrites regulates local gene translation, a key event underlying homeostatic synaptic
380 plasticity [38] .

381 How does elevated RA decrease voltage-gated Ca^{2+} current and synaptic transmission? The size of the Ca^{2+} current in
382 ON-BCs is reduced by photoreceptor degeneration, but the activation and inactivation properties are unchanged,
383 suggesting a decreased level of channel protein rather than a change in channel type. RAR is an enhancer of gene
384 transcription, which often results in increased expression of specific proteins. However, there are many examples of RA-
385 induced down-regulation of proteins, mediated by a sign-inverting gene regulatory cascade [39].

386 L-type Ca^{2+} channels are complexed with accessory proteins, including alpha-2/delta subunits that determine Ca^{2+}
387 current density and activation/inactivation kinetics [40], in addition to controlling vesicle release probability at synapses [41].
388 It is possible that functional down-regulation of Ca^{2+} channels is caused by misregulation of alpha-2/delta, as occurs in
389 sensory neurons in dorsal root ganglia after nerve injury [42]. Many other RA-induced biochemical events could also result
390 in decreased Ca^{2+} current, including altered post-translational modification or altered membrane trafficking of Ca^{2+}
391 channel proteins [42].

392 Is the loss of Ca^{2+} channels sufficient to account for the decline in synaptic release, without invoking additional changes
393 in the release machinery? We find no decline in the number of synaptic contacts between BCs and RGCs and no loss of
394 synaptic ribbons, a key component of the BC synaptic machinery. Hence, at least at this age (p60) in rd1 mice,
395 photoreceptor degeneration causes no obvious structural changes in the BC output synapse. We did observe one
396 interesting phenomenon concerning the frequency-dependence of the ON-BC output synapse in the degenerated retina,
397 but it also may be explained by decreased Ca^{2+} influx during stimulation. We found that paired-pulse depression was
398 dramatically decreased in rd1 and rd10 retinas (Fig. 4f), whereas there was a great increase in failure of the synapse with
399 more sustained, high-frequency stimulation (Fig. 7h). Intracellular Ca^{2+} regulates synaptic vesicle fusion to the plasma
400 membrane, but it is also thought to regulate other steps in the synaptic vesicle cycle, such as vesicle docking and priming
401 [43]. In fact, there is evidence for multiple Ca^{2+}-dependent steps in the vesicle cycle at BC ribbon synapses [31]. If Ca^{2+} influx
402 were sufficient to cause vesicle fusion but insufficient to accelerate vesicle resupply, repetitive stimulation might deplete
403 the pool of readily releasable vesicles before they could be replenished. Different isoforms of synaptotagmin mediate
404 fusion and resupply [44], providing opportunities for understanding how reduced Ca^{2+} influx in remodeled BCs affects
405 synaptic transmission at the molecular level.

406 **Functional impact**

407 Our results imply that physiological remodeling of ON-BCs will constrain information processing further along in the
408 visual system, limiting visual perception. The deficit in temporal coding caused by decreased ON-BC output was

409 particularly severe, which is expected to have a particularly large impact on perception of object motion. Humans with
410 RP often fail to detect moving objects or report motion in the opposite direction of actual movement [45], even if they
411 retain significant visual acuity for detecting static objects [46]. RP is a progressive disease that causes gradual vision loss,
412 but the distinct contributions of decreased photoreceptor density vs. physiological remodeling to vision decline is
413 unclear. Our previous results [9] showed that treatments that reverse physiological remodeling could substantially rescue
414 visual contrast sensitivity in rd10 mice at 2-3 months of age, when photoreceptor degeneration is already severe. We
415 now know that physiological remodeling applies not only to RGCs, but also to BCs, but whether remodeling of one cell
416 type or the other predominates in altering visual perception is also unknown.

417 In certain respects, the physiological remodeling that we characterized in ON-BCs might be considered a homeostatic
418 mechanism, analogous to other compensatory events caused by partial photoreceptor loss (Lee et al., 2022). In the
419 healthy retina, photoreceptors tonically release glutamate, which keeps ON-BCs hyperpolarized. Hypothetically, by
420 eliminating glutamate release, photoreceptor death should depolarize the ON-BCs, chronically activating their voltage-
421 gated Ca^{2+} channels, and increasing their tonic release of glutamate onto RGCs. If this chronic synaptic excitation of RGCs
422 were sufficient to trigger firing, it could impair encoding of synaptic information from other BCs that had yet to undergo
423 remodeling. One way that ON-BCs could compensate for excessive depolarization is by down-regulating their Ca^{2+}
424 channels. While the loss of Ca^{2+} channels might be adaptive, by preventing excessive output from ON-BCs, it comes at a
425 cost. We have demonstrated that physiological remodeling limits the dynamic range of the synaptic output of CBC6 cells
426 (Fig. 2c) and RBCs (Fig. 3c) and severely limits temporal reliability (Fig. 7), maladaptive for encoding visual information.
427 The degree of photoreceptor loss may determine whether physiological remodeling is adaptive or maladaptive.

428 Our findings that physiological remodeling in ON-BCs, as well as RGCs, can be reversed by inhibiting RA has important
429 implications for reviving sight in low-vision patients with RP and perhaps other photoreceptor degenerative disorders.
430 They also have important implications for vision restoration in advanced RP patients with nearly complete
431 photoreceptor loss and little remaining light perception. One treatment approach for these patients is to install light
432 responses in surviving neurons of the outer retina, including ON-BCs, either through optogenetic stimulation [6,47] or
433 electrical stimulation with sub-retinal implants [48]. Physiological remodeling of the ON-BC output synapse is predicted to
434 seriously limit the effectiveness of direct or indirect stimulation of BCs on downstream information processing and visual
435 perception. Our results indicate that reduced frequency-response of the ON-BC output synapse, seen as a failure of
436 EPSCs, severely impairs RGC spike-rate coding. In the clinical context, this may severely limit the effectiveness of
437 optogenetic therapies targeted to ON-BCs or upstream remnant photoreceptors in degenerated retina. The same
438 problems may also apply to signals initiated by stem-cell derived regenerated photoreceptors inserted into the outer
439 retina. Inhibiting RA synthesis or signaling may remove these problems and augment the effectiveness of any vision
440 restoration technology that delivers light-elicited signals to the blind retina. RA inhibition can be accomplished with
441 pharmacological inhibitors of RALDH or RAR [9], or with targeted AAV vectors that deliver genetic-based inhibitors of
442 RALDH and RAR to specific retinal cell types, for example ON-BCs or RGCs [5,47].

443 Methods

444 **Animals**

445 Mice were handled in accordance with protocols approved by the UC Berkeley Institutional Animal Care and Use
446 Committee (AUP-2016-04-8700-1) and conformed to the NIH Guide for the Care and Use of Laboratory Animals.
447 C3H/HeJ mice (Jackson 000659) were used as the rd1 model (*Pde6b*^{rd1}). B6.CXB1-Pde6b^{rd10}/J mice were used as the rd10
448 model (Jackson 004297). CCK-ires-Cre knock-in mice (Jackson 012706, abbreviated CCK-Cre) were used to drive Cre
449 recombinase under the cholecystokinin promoter to label CBC6 cells. BAC-Pcp2-IRES-Cre mice (Jackson 010536,
450 abbreviated Pcp2-Cre) were used to drive Cre recombinase under the Pcp2 promoter to label RBCs. Ai32 mice (Jackson
451 024109, B6.Cg-*Gt(ROSA)26Sor*$^{tm32(CAG-COP4*H134R/EYFP)Hze}$/J) were used to drive channelrhodopsin-2/eYFP fusion protein in
452 Cre-expressing CBC6 or RBC cells. Both rd1 and rd10 mice strains were homozygous for their respective mutations in the
453 *Pde6b* locus. The CCK-Cre, Pcp2-Cre, and Ai32 alleles were always used in mice in a hemizygous state. Mice of both sexes
454 were used interchangeably. For experiments with WT and rd1 mice, animals were used within 3 days of postnatal day 60
455 (p60). For experiments with rd10 mice, animals were used within 3 days of p90.

456 **Retinal Dissection**

457 Mice were euthanized via isoflurane exposure and internal decapitation. Retinal dissection was performed with
458 enucleated eyes in oxygenated ACSF (in mM: 119 NaCl, 26.2 $NaHCO_3$, 11 Dextrose, 2.5 KCl mM, 1 K_2HPO_4, 1.3 $MgCl_2$*
459 $6H_2O$, 2.5 $CaCl_2$, 293 mOsm/Kg), (5% CO_2/95% O_2) in room light conditions with a dissection microscope. For retinal
460 whole-mount experiments, retinas were flattened with 4 relieving cuts. For retinal slice experiments, flattened retinas
461 were mounted on 13 mm diameter 0.45 µm filter paper discs (MF-Millipore) and sliced to a thickness of 250 µm with a
462 Stoelting Tissue Slicer. Retinal slices were rotated 90 degrees and mounted within a vacuum grease well.

463 **Electrophysiology**

464 For RGC recordings, retinas were isolated and incubated in ACSF containing hyaluronidase (9,800 U/mL) and collagenase
465 (2,500 U/mL) for 10 minutes to facilitate penetrating of the inner limiting membrane allowing access to RGC somas for
466 patch clamp recording [49]. Retinas were mounted ganglion cell side up in a recording chamber and held in place with a
467 harp (Warner Instruments), superfused with ACSF oxygenated with 5% CO_2/95% O_2 at a rate of 5 ml/minute at 34
468 degrees C and viewed under DIC optics with an upright microscope (Olympus). Reagents for ACSF were purchased from
469 Fisher Scientific.

470 For retinal slice experiments, slices were made as described and perfused in the same way as whole-mount retinas.
471 Electrodes were made with boroscilicate capillary glass tubing with OD = 1.5 mm, ID = 1.17 mm (Warner G150TF-4). For
472 RGC recording, glass was pulled to a resistance of 5-6 MΩs using a Narishige pipette puller. For BCs and amacrine cell
473 recording, electrodes were made with a resistance of 7-8 MΩs with a Sutter Instruments P1000. For voltage clamp

474 experiments, the pipette solution contained (in mM): 123 Cs gluconate, 8 NaCl, 1 $CaCl_2$, 10 EGTA, 10 HEPES, 10 glucose,
475 5 Mg^{2+} ATP, 5 QX 314 (Tocris Bioscience), 0.01 Alexa 594, pH 7.4 with CsOH, 293 mOsm/Kg. For current clamp
476 experiments in BCs to measure optogenetic responses, the pipette solution contained (in mM): 125 K^+ Gluconate, 10
477 EGTA, 10 KCl, 10 HEPES, 4 Mg^{2+} ATP, 0.01 Alexa 594, 293 mOsm/Kg. Alexa Fluor 594 Hydrazide (ThermoFisher Scientific)
478 at 10 µM was used to dye fill all cells during recording for confirmation of cell identity. Whole cell recordings were
479 sampled at 20 kHz and filtered at 2 kHz with a Multiclamp 700B amplifier, digitized with a 1440a or 1550a Digidata A-D
480 converter and analyzed offline with Axograph X or Clampfit. Recordings with series resistance above 10% of the cell
481 membrane resistance or reached above 30 mΩ were discarded.

482 To block photoreceptor responses to light, the kainate receptor antagonist ACET (1 µM) and the mGluR6 agonist L-AP4
483 (10 µM) were added to ACSF. Gabazine (10 µM) and strychnine (10 µM) were also added to block ionotropic GABA and
484 glycine receptors. MFA (100 µM) was used to inhibit gap junctions. Pharmacological agents were purchased from Tocris
485 Biosciences.

486 Optogenetic stimulation of CBC6s and RBCs was provided by a 470 nm LED delivering $2.1X10^8$ photons/s, (Lumencore or
487 CoolLED pE-4000) measured at the plane of the retina with a spectrophotometer (Thor Labs). For figures 2 and 3,
488 stimulation intensity was varied by changing the duration of the stimulus from 0.1 to 10 ms. Thus, the number of
489 photons delivered during the optogenetic stimulus ranged from $2.1X10^7$ (100%) to $2.1X10^5$ (1%).

490 **Mapping ON α-RGC Virtual Spatial Receptive Rield**

491 Spots of light with a 50 µm diameter were generated with a Texas Instruments Digital Light Projector (CEL1015 Light
492 Engine, Digital Light innovations) controlled with CELconductor Control Software. Briefly, an ON α-RGC was identified
493 and patch clamped as described above. The cell body was focused on with an Olympus LUMPlanFl 20x/0.5 W ∞/0
494 objective and centered within a 650 µm x 650 µm field of view. Each spot projection and simultaneous EPSC recording
495 was controlled via Digidata.

496 **Trans-Retinal Stimulation**

497 To achieve electrical trans-retinal stimulation, a custom chamber was created. A 65 mm petri dish was shaved down in
498 height and embedded within a 100 mm petri dish with RTV sealant. The 65 mm dish was elevated ~ 3 mm from the
499 bottom of the 100 mm dish. An approximately 1 mm hole was melted in the center of the 65 mm dish with a 21 gauge
500 needle. To mount a retina, a ~ 7.5 mm x 7.5 mm piece of ion-permeant dialysis membrane was placed over the 1 mm
501 hole to supply an even surface to place a flat-mount retina, RGC side up. A ~ 7.5 mm x 7.5 mm piece of flexible
502 cellophane with an ~ 1mm hole punched into the center was placed over the retina as a coverslip. The retina is then
503 sealed between the membrane and coverslip with vacuum grease so that the only electrical path between the two
504 dishes is through the retina. Two copper wires were placed in each dish below and above the retina which were

505 connected to an ISO-Flex stimulus isolation unit. Electrical stimulation was achieved by setting the desired voltage on
506 the ISO-Flex and triggering the stimulus via Digidata.

507 **2-Photon iGluSnFR Imaging**

508 2-Photon fluorescence imaging was performed on a Sutter Instruments moveable objective microscope with an Olympus
509 XLUMPlanFl 20x/0.95 W ∞/0 objective. iGluSnFR excitation was achieved with a Coherent Chameleon Ultra II tuned to
510 910 nm. Imaging was performed with ScanImage software. Scanning field of view was 25 µm x 25 µm. Images collected
511 in Fig 4c-d were scanned at 256 pixels per line x 256 lines (frame rate = 1.48 Hz, 2 ms per line). Higher time resolution of
512 iGluSnFR flouresence for Fig 4e-g was performed at 256 pixels per line x 6 lines (frame rate = 63.13 Hz, 2 ms per line).

513 **Immunohistochemistry**

514 ON α-RGCs were injected with Alexa Fluor 568 hydrazide (A10441, Thermo Fisher) as described previously [50]. In short,
515 somas of RGCs in the whole-mount retina were visualized by acridine orange labeling [51]. Potential ON α-RGCs were
516 identified based on their large soma size (>20 µm) and targeted with sharp microelectrodes containing Alexa Fluor 568.
517 The dye injected retinas were fixed with 4% PFA and the following immunolabeling was carried out as described before
518 [52] . In brief, the whole-mount retinas were incubated into primary and secondary antibodies for 3 and 1 days,
519 respectively. CtBP2 (mouse, AB_399431, BD Biosciences) monoclonal and secretagogin (sheep, AB_2034062, BioVendor)
520 polyclonal antibodies were used at a dilution of 1:500 and 1:750, respectively. All immunostainings were performed at
521 room temperature. Images were scanned with 40x/1.4 oil objective using Zeiss LSM780 Laser Scanning Confocal
522 Microscope. The z-stacks were acquired at a constant pixel size of 60nm*60nm and a z-step of 0.3µm unless stated
523 otherwise. All raw images thus obtained were deconvolved with Huygens Essential software (Scientific Volume Imaging,
524 Netherlands). The deconvolution was achieved by using a theoretical point spread function. The resulting images were
525 further processed and analyzed in Fiji (https://fiji.sc/) [53]. The z-stacks were normalized using stack histograms prior to
526 analysis. The colocalization analysis was carried out within each optical section unless stated otherwise. Brightness and
527 contrast of the images were adjusted post-analysis in Fiji.

528 Colocalization between channels was performed with Fiji utilizing the colocalization highlighter plugin as previously
529 described [54]. Briefly, deconvoluted z-stacks were segmented using stack histogram. Secretagogin and CtBP2 signals were
530 thresholded with Otsu's method, and dye injected RGCs were manually thresholded. With colocalization highlighter, an
531 intensity ratio of 50% was applied to estimate colocalization between Secretagogin and CtBP2. Colocalization of
532 Secretagogin and CtBP2 with RGCs was performed sequentially with an intensity ratio of 10%. Resultant 8-bit images of
533 puncta were generated where at least 5 or more connected voxels were considered as colocalization. These images
534 were overlayed with either RGCs or CBC6 axon terminals, and the 3D Objects Counter plugin was used to quantify
535 putative synaptic contacts. To isolate individual CBC6 axon terminals, axonal endings were traced back from a common
536 point in the z-stack 8 µm into the IPL.

537 **AAV Delivery of iGluSnFR**

538 Plasmid containing iGluSnFR(A184S) under the control of the human synapsin promoter was purchased from Addgene
539 (#106174) and packaged in the AAV8-Y733F serotype [55]. Viral constructs were generated in the Gene Delivery module of
540 the Vision Science Core at UC Berkeley. One month prior to imaging, 1.5 μl of virus ($1x10^{15}$ vg/mL) was injected into
541 intravitreally into the eye of rd1 or WT mice.

542 **Data Visualization and Statistics**

543 All reported statistics and diagrams were generated with R 4.2.2. Retinal and experimental diagrams were created with
544 Biorender.com.

545

546 References

547 1. Mazzoni, F., Novelli, E., and Strettoi, E. (2008). Retinal ganglion cells survive and maintain normal dendritic
548 morphology in a mouse model of inherited photoreceptor degeneration. The Journal of neuroscience : the
549 official journal of the Society for Neuroscience *28*, 14282-14292. 10.1523/JNEUROSCI.4968-08.2008.
550 2. Medeiros, N.E., and Curcio, C.A. (2001). Preservation of ganglion cell layer neurons in age-related macular
551 degeneration. Investigative ophthalmology & visual science *42*, 795-803.
552 3. Ellis, E.M., Paniagua, A.E., Scalabrino, M.L., Thapa, M., Rathinavelu, J., Jiao, Y., Williams, D.S., Field, G.D., Fain,
553 G.L., and Sampath, A.P. (2023). Cones and cone pathways remain functional in advanced retinal degeneration.
554 Current biology : CB *33*, 1513-1522.e1514. 10.1016/j.cub.2023.03.007.
555 4. Humayun, M.S., Dorn, J.D., da Cruz, L., Dagnelie, G., Sahel, J.A., Stanga, P.E., Cideciyan, A.V., Duncan, J.L., Eliott,
556 D., Filley, E., et al. (2012). Interim results from the international trial of Second Sight's visual prosthesis.
557 Ophthalmology *119*, 779-788. 10.1016/j.ophtha.2011.09.028.
558 5. Bi, A., Cui, J., Ma, Y.P., Olshevskaya, E., Pu, M., Dizhoor, A.M., and Pan, Z.H. (2006). Ectopic expression of a
559 microbial-type rhodopsin restores visual responses in mice with photoreceptor degeneration. Neuron *50*, 23-33.
560 10.1016/j.neuron.2006.02.026.
561 6. Sahel, J.A., Boulanger-Scemama, E., Pagot, C., Arleo, A., Galluppi, F., Martel, J.N., Esposti, S.D., Delaux, A., de
562 Saint Aubert, J.B., de Montleau, C., et al. (2021). Partial recovery of visual function in a blind patient after
563 optogenetic therapy. Nature medicine *27*, 1223-1229. 10.1038/s41591-021-01351-4.
564 7. Polosukhina, A., Litt, J., Tochitsky, I., Nemargut, J., Sychev, Y., De Kouchkovsky, I., Huang, T., Borges, K., Trauner,
565 D., Van Gelder, R.N., and Kramer, R.H. (2012). Photochemical restoration of visual responses in blind mice.
566 Neuron *75*, 271-282. 10.1016/j.neuron.2012.05.022.
567 8. Tochitsky, I., Polosukhina, A., Degtyar, V.E., Gallerani, N., Smith, C.M., Friedman, A., Van Gelder, R.N., Trauner,
568 D., Kaufer, D., and Kramer, R.H. (2014). Restoring visual function to blind mice with a photoswitch that exploits
569 electrophysiological remodeling of retinal ganglion cells. Neuron *81*, 800-813. 10.1016/j.neuron.2014.01.003.
570 9. Telias, M., Sit, K.K., Frozenfar, D., Smith, B., Misra, A., Goard, M.J., and Kramer, R.H. (2022). Retinoic acid
571 inhibitors mitigate vision loss in a mouse model of retinal degeneration. Science advances *8*, eabm4643.
572 10.1126/sciadv.abm4643.
573 10. Pfeiffer, R.L., Marc, R.E., and Jones, B.W. (2020). Persistent remodeling and neurodegeneration in late-stage
574 retinal degeneration. Progress in retinal and eye research *74*, 100771. 10.1016/j.preteyeres.2019.07.004.
575 11. Stasheff, S.F., Shankar, M., and Andrews, M.P. (2011). Developmental time course distinguishes changes in
576 spontaneous and light-evoked retinal ganglion cell activity in rd1 and rd10 mice. Journal of neurophysiology *105*,
577 3002-3009. 10.1152/jn.00704.2010.

578 12. Telias, M., Denlinger, B., Helft, Z., Thornton, C., Beckwith-Cohen, B., and Kramer, R.H. (2019). Retinoic Acid
579 Induces Hyperactivity, and Blocking Its Receptor Unmasks Light Responses and Augments Vision in Retinal
580 Degeneration. Neuron *102*, 574-586 e575. 10.1016/j.neuron.2019.02.015.
581 13. Tochitsky, I., Helft, Z., Meseguer, V., Fletcher, R.B., Vessey, K.A., Telias, M., Denlinger, B., Malis, J., Fletcher, E.L.,
582 and Kramer, R.H. (2016). How Azobenzene Photoswitches Restore Visual Responses to the Blind Retina. Neuron
583 *92*, 100-113. 10.1016/j.neuron.2016.08.038.
584 14. Marc, R.E., Jones, B.W., Watt, C.B., and Strettoi, E. (2003). Neural remodeling in retinal degeneration. Progress in
585 retinal and eye research *22*, 607-655. 10.1016/s1350-9462(03)00039-9.
586 15. Dunn, F.A. (2015). Photoreceptor ablation initiates the immediate loss of glutamate receptors in postsynaptic
587 bipolar cells in retina. The Journal of neuroscience : the official journal of the Society for Neuroscience *35*, 2423-
588 2431. 10.1523/JNEUROSCI.4284-14.2015.
589 16. Gayet-Primo, J., and Puthussery, T. (2015). Alterations in Kainate Receptor and TRPM1 Localization in Bipolar
590 Cells after Retinal Photoreceptor Degeneration. Front Cell Neurosci *9*, 486. 10.3389/fncel.2015.00486.
591 17. Lin, Y., Jones, B.W., Liu, A., Tucker, J.F., Rapp, K., Luo, L., Baehr, W., Bernstein, P.S., Watt, C.B., Yang, J.H., et al.
592 (2012). Retinoid receptors trigger neuritogenesis in retinal degenerations. FASEB journal : official publication of
593 the Federation of American Societies for Experimental Biology *26*, 81-92. 10.1096/fj.11-192914.
594 18. Care, R.A., Kastner, D.B., De la Huerta, I., Pan, S., Khoche, A., Della Santina, L., Gamlin, C., Santo Tomas, C., Ngo,
595 J., Chen, A., et al. (2019). Partial Cone Loss Triggers Synapse-Specific Remodeling and Spatial Receptive Field
596 Rearrangements in a Mature Retinal Circuit. Cell reports *27*, 2171-2183.e2175. 10.1016/j.celrep.2019.04.065.
597 19. Shen, N., Wang, B., Soto, F., and Kerschensteiner, D. (2020). Homeostatic Plasticity Shapes the Retinal Response
598 to Photoreceptor Degeneration. Current biology : CB *30*, 1916-1926.e1913. 10.1016/j.cub.2020.03.033.
599 20. Tachibana, M., Okada, T., Arimura, T., Kobayashi, K., and Piccolino, M. (1993). Dihydropyridine-sensitive calcium
600 current mediates neurotransmitter release from bipolar cells of the goldfish retina. The Journal of Neuroscience
601 *13*, 2898-2909. 10.1523/jneurosci.13-07-02898.1993.
602 21. Heidelberger, R., and Matthews, G. (1992). Calcium influx and calcium current in single synaptic terminals of
603 goldfish retinal bipolar neurons. J Physiol *447*, 235-256. 10.1113/jphysiol.1992.sp019000.
604 22. Tien, N.-W., Soto, F., and Kerschensteiner, D. (2017). Homeostatic Plasticity Shapes Cell-Type-Specific Wiring in
605 the Retina. Neuron *94*, 656-665.e654. 10.1016/j.neuron.2017.04.016.
606 23. Zhu, Y., Xu, J., Hauswirth, W.W., and DeVries, S.H. (2014). Genetically targeted binary labeling of retinal neurons.
607 The Journal of neuroscience : the official journal of the Society for Neuroscience *34*, 7845-7861.
608 10.1523/JNEUROSCI.2960-13.2014.
609 24. Liang, C.-Q., Zhang, G., Zhang, L., Chen, S.-Y., Wang, J.-N., Zhang, T.-T., Singer, J.H., and Ke, J.-B. (2021).
610 Calmodulin Bidirectionally Regulates Evoked and Spontaneous Neurotransmitter Release at Retinal Ribbon
611 Synapses. eneuro *8*, ENEURO.0257-0220.2020. 10.1523/eneuro.0257-20.2020.

612 25. Singer, J.H., Lassová, L., Vardi, N., and Diamond, J.S. (2004). Coordinated multivesicular release at a mammalian
613 ribbon synapse. Nature Neuroscience *7*, 826-833. 10.1038/nn1280.
614 26. Puthussery, T., Gayet-Primo, J., and Taylor, W.R. (2010). Localization of the calcium-binding protein secretagogin
615 in cone bipolar cells of the mammalian retina. The Journal of comparative neurology *518*, 513-525.
616 10.1002/cne.22234.
617 27. Schwartz, G.W., Okawa, H., Dunn, F.A., Morgan, J.L., Kerschensteiner, D., Wong, R.O., and Rieke, F. (2012). The
618 spatial structure of a nonlinear receptive field. Nat Neurosci *15*, 1572-1580. 10.1038/nn.3225.
619 28. Helmstaedter, M., Briggman, K.L., Turaga, S.C., Jain, V., Seung, H.S., and Denk, W. (2013). Connectomic
620 reconstruction of the inner plexiform layer in the mouse retina. Nature *500*, 168-174. 10.1038/nature12346.
621 29. Germain, P., Gaudon, C., Pogenberg, V., Sanglier, S., Van Dorsselaer, A., Royer, C.A., Lazar, M.A., Bourguet, W.,
622 and Gronemeyer, H. (2009). Differential Action on Coregulator Interaction Defines Inverse Retinoid Agonists and
623 Neutral Antagonists. Chemistry & Biology *16*, 479-489. https://doi.org/10.1016/j.chembiol.2009.03.008.
624 30. Singer, J.H., and Diamond, J.S. (2006). Vesicle depletion and synaptic depression at a mammalian ribbon
625 synapse. Journal of neurophysiology *95*, 3191-3198. 10.1152/jn.01309.2005.
626 31. Gomis, A., Burrone, J., and Lagnado, L. (1999). Two actions of calcium regulate the supply of releasable vesicles
627 at the ribbon synapse of retinal bipolar cells. The Journal of neuroscience : the official journal of the Society for
628 Neuroscience *19*, 6309-6317. 10.1523/jneurosci.19-15-06309.1999.
629 32. Scalabrino, M.L., Thapa, M., Chew, L.A., Zhang, E., Xu, J., Sampath, A.P., Chen, J., and Field, G.D. (2022). Robust
630 cone-mediated signaling persists late into rod photoreceptor degeneration. Elife *11*. 10.7554/eLife.80271.
631 33. Sekirnjak, C., Jepson, L.H., Hottowy, P., Sher, A., Dabrowski, W., Litke, A.M., and Chichilnisky, E.J. (2011). Changes
632 in physiological properties of rat ganglion cells during retinal degeneration. Journal of neurophysiology *105*,
633 2560-2571. 10.1152/jn.01061.2010.
634 34. Trenholm, S., and Awatramani, G.B. (2015). Origins of spontaneous activity in the degenerating retina. Frontiers
635 in Cellular Neuroscience *9*. 10.3389/fncel.2015.00277.
636 35. Choi, H., Zhang, L., Cembrowski, M.S., Sabottke, C.F., Markowitz, A.L., Butts, D.A., Kath, W.L., Singer, J.H., and
637 Riecke, H. (2014). Intrinsic bursting of AII amacrine cells underlies oscillations in the rd1 mouse retina. Journal of
638 neurophysiology *112*, 1491-1504. 10.1152/jn.00437.2014.
639 36. Harper, A.R., Wiechmann, A.F., Moiseyev, G., Ma, J.X., and Summers, J.A. (2015). Identification of active
640 retinaldehyde dehydrogenase isoforms in the postnatal human eye. PloS one *10*, e0122008.
641 10.1371/journal.pone.0122008.
642 37. McCaffery, P., Mey, J., and Dräger, U.C. (1996). Light-mediated retinoic acid production. Proc Natl Acad Sci U S A
643 *93*, 12570-12574. 10.1073/pnas.93.22.12570.
644 38. Thapliyal, S., Arendt, K.L., Lau, A.G., and Chen, L. (2022). Retinoic acid-gated BDNF synthesis in neuronal
645 dendrites drives presynaptic homeostatic plasticity. Elife *11*. 10.7554/eLife.79863.

646 39. Balmer, J.E., and Blomhoff, R. (2002). Gene expression regulation by retinoic acid. Journal of Lipid Research *43*,
647 1773-1808. 10.1194/jlr.R100015-JLR200.
648 40. Dolphin, A.C. (2009). Calcium channel diversity: multiple roles of calcium channel subunits. Current opinion in
649 neurobiology *19*, 237-244. 10.1016/j.conb.2009.06.006.
650 41. Hoppa, M.B., Lana, B., Margas, W., Dolphin, A.C., and Ryan, T.A. (2012). α2δ expression sets presynaptic calcium
651 channel abundance and release probability. Nature *486*, 122-125. 10.1038/nature11033.
652 42. D'Arco, M., Margas, W., Cassidy, J.S., and Dolphin, A.C. (2015). The upregulation of α2δ-1 subunit modulates
653 activity-dependent Ca2+ signals in sensory neurons. The Journal of neuroscience : the official journal of the
654 Society for Neuroscience *35*, 5891-5903. 10.1523/jneurosci.3997-14.2015.
655 43. Wan, Q.F., and Heidelberger, R. (2011). Synaptic release at mammalian bipolar cell terminals. Visual
656 neuroscience *28*, 109-119. 10.1017/S0952523810000453.
657 44. Weingarten, D.J., Shrestha, A., Juda-Nelson, K., Kissiwaa, S.A., Spruston, E., and Jackman, S.L. (2022). Fast
658 resupply of synaptic vesicles requires synaptotagmin-3. Nature *611*, 320-325. 10.1038/s41586-022-05337-1.
659 45. Turano, K., and Wang, X. (1992). Motion thresholds in retinitis pigmentosa. Investigative ophthalmology & visual
660 science *33*, 2411-2422.
661 46. Alexander, K.R., Derlacki, D.J., Xie, W., Fishman, G.A., and Szlyk, J.P. (1998). Discrimination of spatial
662 displacements by patients with retinitis pigmentosa. Vision research *38*, 1171-1181.
663 https://doi.org/10.1016/S0042-6989(97)00235-6.
664 47. Lagali, P.S., Balya, D., Awatramani, G.B., Münch, T.A., Kim, D.S., Busskamp, V., Cepko, C.L., and Roska, B. (2008).
665 Light-activated channels targeted to ON bipolar cells restore visual function in retinal degeneration. Nat
666 Neurosci *11*, 667-675. 10.1038/nn.2117.
667 48. Roux, S., Matonti, F., Dupont, F., Hoffart, L., Takerkart, S., Picaud, S., Pham, P., and Chavane, F. (2016). Probing
668 the functional impact of sub-retinal prosthesis. Elife *5*. 10.7554/eLife.12687.
669 49. Schmidt, T.M., and Kofuji, P. (2011). An Isolated Retinal Preparation to Record Light Response from Genetically
670 Labeled Retinal Ganglion Cells. JoVE, e2367. doi:10.3791/2367.
671 50. Tetenborg, S., Yadav, S.C., Hormuzdi, S.G., Monyer, H., Janssen-Bienhold, U., and Dedek, K. (2017). Differential
672 Distribution of Retinal Ca(2+)/Calmodulin-Dependent Kinase II (CaMKII) Isoforms Indicates CaMKII-β and -δ as
673 Specific Elements of Electrical Synapses Made of Connexin36 (Cx36). Frontiers in molecular neuroscience *10*,
674 425. 10.3389/fnmol.2017.00425.
675 51. Meyer, A., Yadav, S. C., and Dedek, K. (2018). Phenotyping of gap-junctional coupling in the mouse retina.
676 Methods Mol. Biol. 1753, 249–259. doi: 10.1007/978-1-4939-7720-8_17.
677 52. Yadav, S.C., Tetenborg, S., and Dedek, K. (2019). Gap Junctions in A8 Amacrine Cells Are Made of Connexin36 but
678 Are Differently Regulated Than Gap Junctions in AII Amacrine Cells. Frontiers in molecular neuroscience *12*, 99.
679 10.3389/fnmol.2019.00099.

680 53. Schindelin, J., Arganda-Carreras, I., Frise, E., Kaynig, V., Longair, M., Pietzsch, T., Preibisch, S., Rueden, C.,
681 Saalfeld, S., Schmid, B., et al. (2012). Fiji: an open-source platform for biological-image analysis. Nat Methods *9*,
682 676-682. 10.1038/nmeth.2019.
683 54. Behrens, C., Yadav, S.C., Korympidou, M.M., Zhang, Y., Haverkamp, S., Irsen, S., Schaedler, A., Lu, X., Liu, Z.,
684 Lause, J., et al. (2022). Retinal horizontal cells use different synaptic sites for global feedforward and local
685 feedback signaling. Current biology : CB *32*, 545-558.e545. 10.1016/j.cub.2021.11.055.
686 55. Dalkara, D., Byrne, L.C., Klimczak, R.R., Visel, M., Yin, L., Merigan, W.H., Flannery, J.G., and Schaffer, D.V. (2013).
687 In vivo-directed evolution of a new adeno-associated virus for therapeutic outer retinal gene delivery from the
688 vitreous. Science translational medicine *5*, 189ra176. 10.1126/scitranslmed.3005708.

689

690 **Supplemental Figures**

691

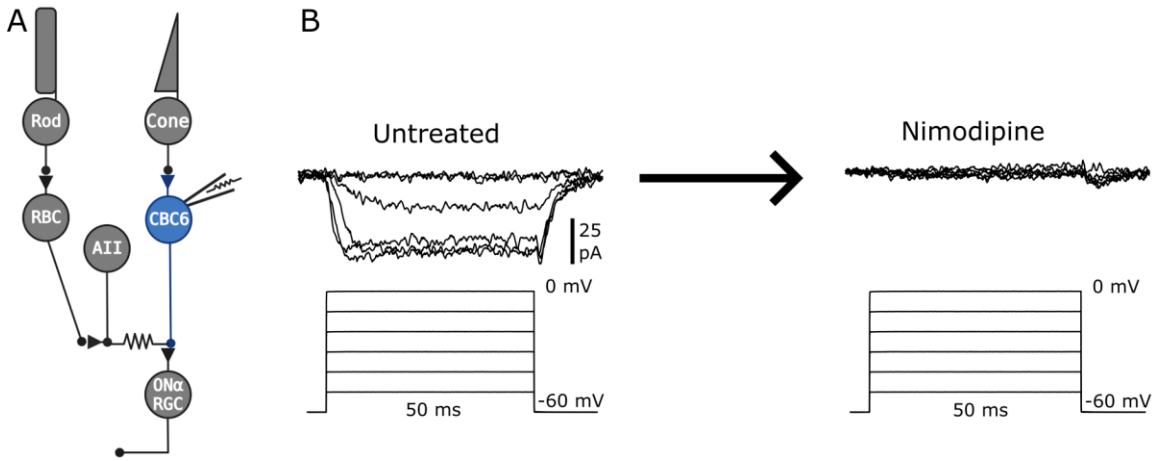

692

693 **Supplemental Figure 1. Voltage-gated Ca^{2+} current is eliminated by the L-type Ca^{2+} channel blocker nimodipine.** A)
694 Retinal circuit diagrams showing whole-cell patch-clamped CBC6 cells. B) Application of 10 µM nimodipine eliminated
695 voltage-gated Ca^{2+} current in a WT cell, indicating the observed voltage-gated Ca^{2+} current is generated by L-type channels
696 in CBC6 cells.

697

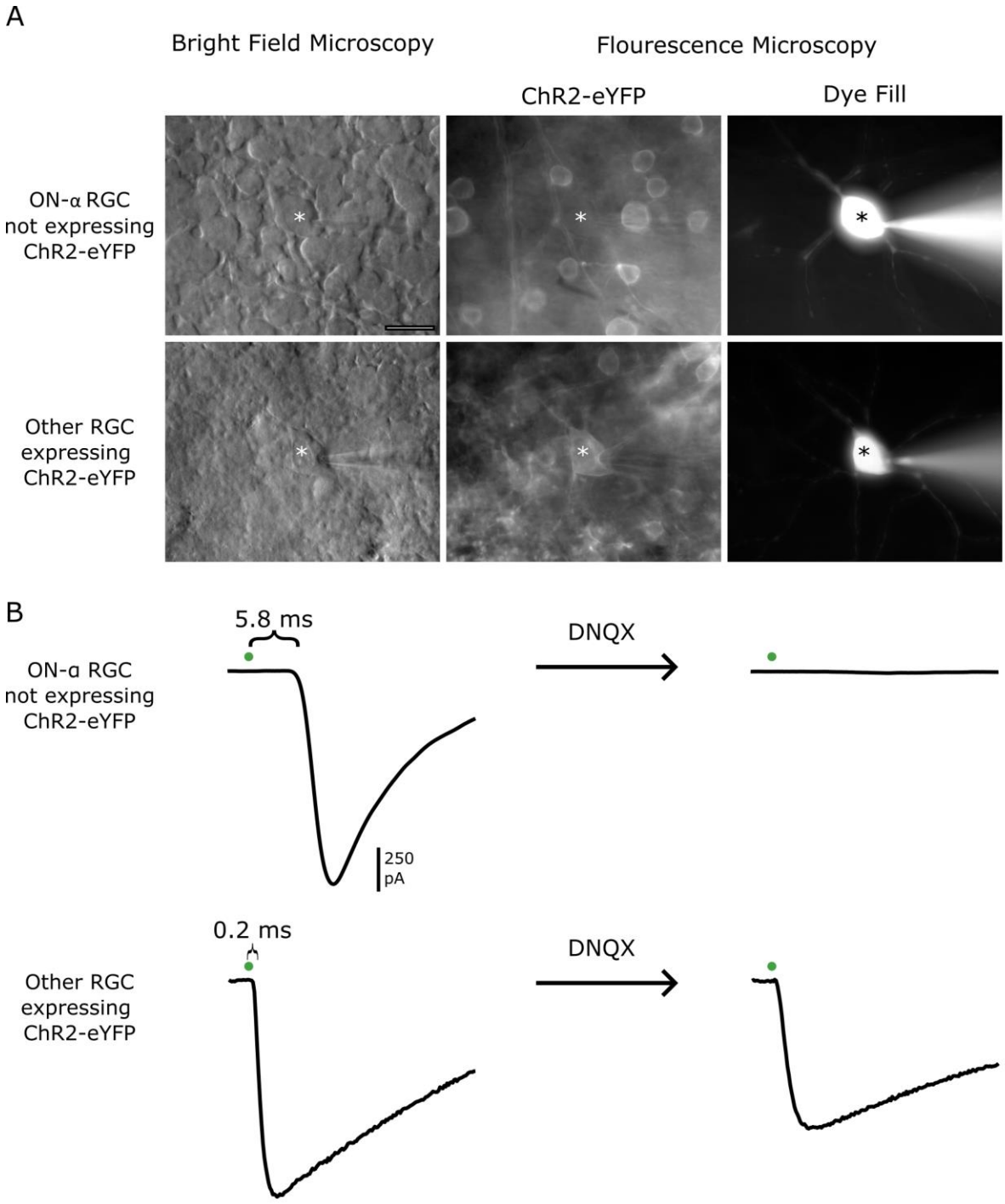

Supplemental Figure 2. ON α-RGCs do not express ChR2-eYFP. A) An ON α-RGC patch clamped using bright field microscopy does not express ChR2-eYFP visualized with fluorescence microscopy. An other RGC, that is not an ON α-RGC, patch clamped using bright field microscopy is expressing ChR2-eYFP visualized with fluorescence microscopy. B) Optogenetic stimulation of ON a-RGCs evoked EPSCs at latencies consistent with monosynaptic transmission. Blocking synaptic transmission with DNQX application fully eliminates the EPSC. Optogenetic stimulation of other ChR2-eYFP expressing RGCS generate currents with extremely short latency that are mostly insensitive to synaptic blockade with DNQX.

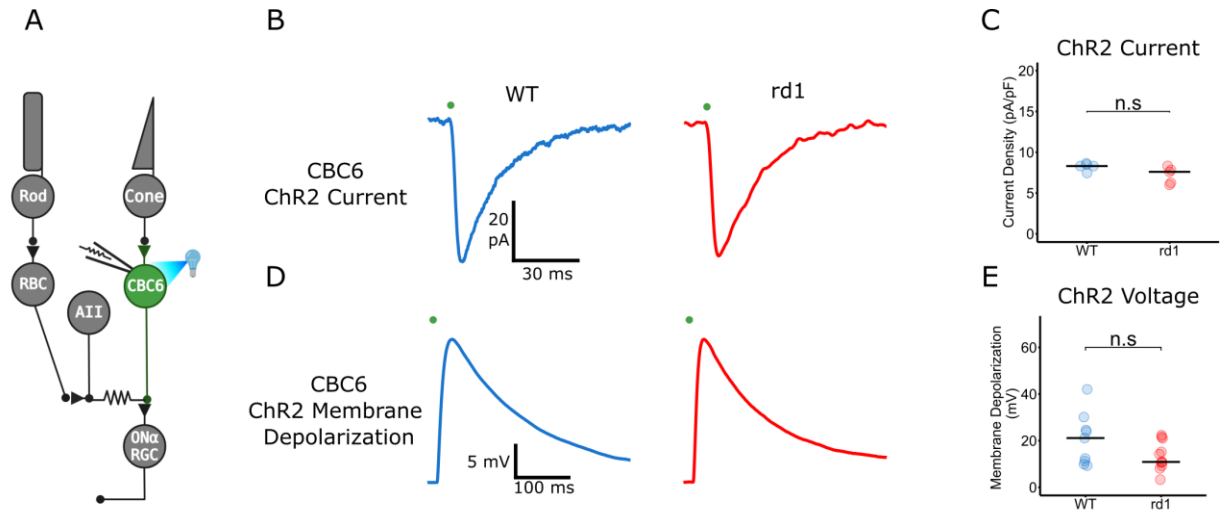

Supplemental Figure 3. CBC6 cells from WT and rd1 retinas have the same ChR2 current density and depolarize the same amount in response to optogenetic light. A) Retinal circuit diagram showing whole-cell patch-clamp and simultaneous optogenetic stimulation of a CBC6 cell. B) ChR2-induced inward current elicited by optogenetic stimulation of CBC6 cells in WT and rd1. C) There is no difference in ChR2 current density in CBC6s in WT and rd1 retinas ($p = 0.15$). D) ChR2-induced membrane depolarization elicited by optogenetic stimulation of CBC6 cells in WT and rd1. E) There is no difference in the magnitude of ChR2-induced depolarization in CBC6s in WT and rd1 retinas ($p = 0.11$). All statistical comparisons were made with PWT with FDR correction.

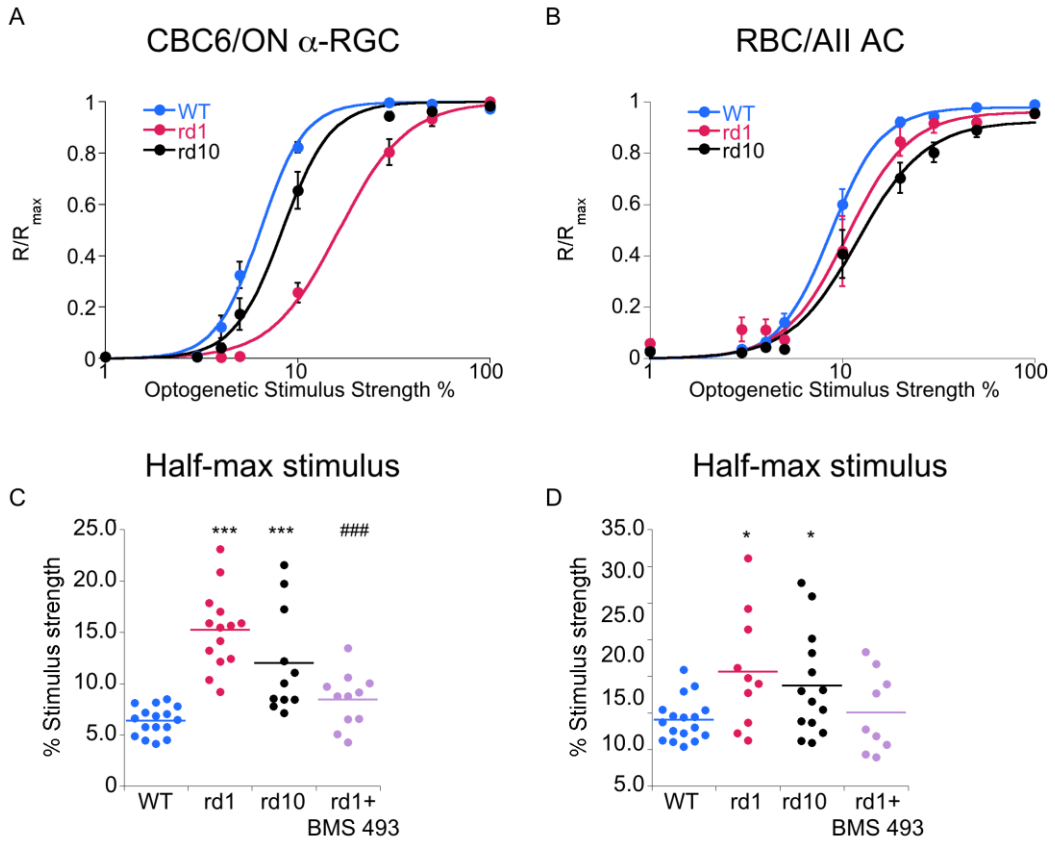

Supplemental Figure 4. Reduced sensitivity of ON bipolar cell synaptic transmission in degenerated retinas. A,B) Stimulus vs. response plots from Fig. 2 scaled to the maximal EPSC response. The shift along the x-axis indicates reduced sensitivity of cone (A) and rod (B) BC synapses in degenerated retinas. C,D) Summary of the stimulus strength required to elicit half-maximal EPSCs in CBC6 (C) and AII ACs (D). In all cases, 100% stimulus strength was a 10 ms 470 nm flash delivering $2.1X10^7$ photons. *** indicates p<0.0001, * indicates p=0.02 rd1 vs. WT, p=0.05 rd10 vs. WT. ### indicates p<0.0001 vs. rd1. All statistical comparisons were made with PWT with FDR correction.

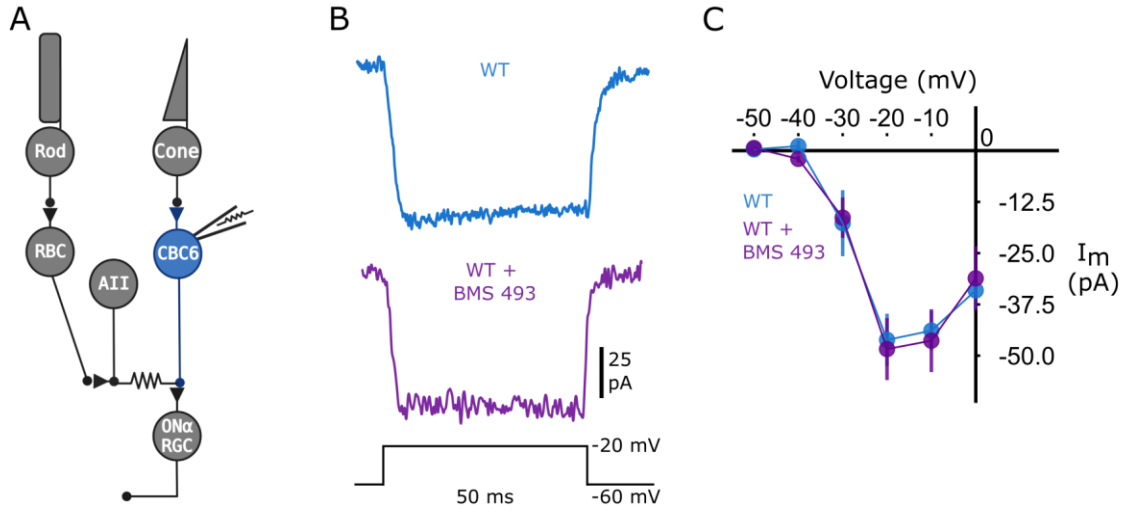

Supplementary Figure 5. BMS 493 does not increase voltage-gated calcium current in WT retina. A) Retinal circuit diagrams showing whole-cell patch-clamped CBC6 cells. B) Inward calcium currents from CBC6 cells from WT and BMS 493-treated retinas. Current was activated with a depolarizing voltage step (50 ms) from -60 mV to -20 mV. C) Steady-state current vs. voltage (I-V) curves, elicited with a series of 10 mV incrementing depolarizing steps from -60 mV. There was no significant difference between WT and BMS 493-treated retinas. All statistical comparisons were made with PWT with FDR correction.

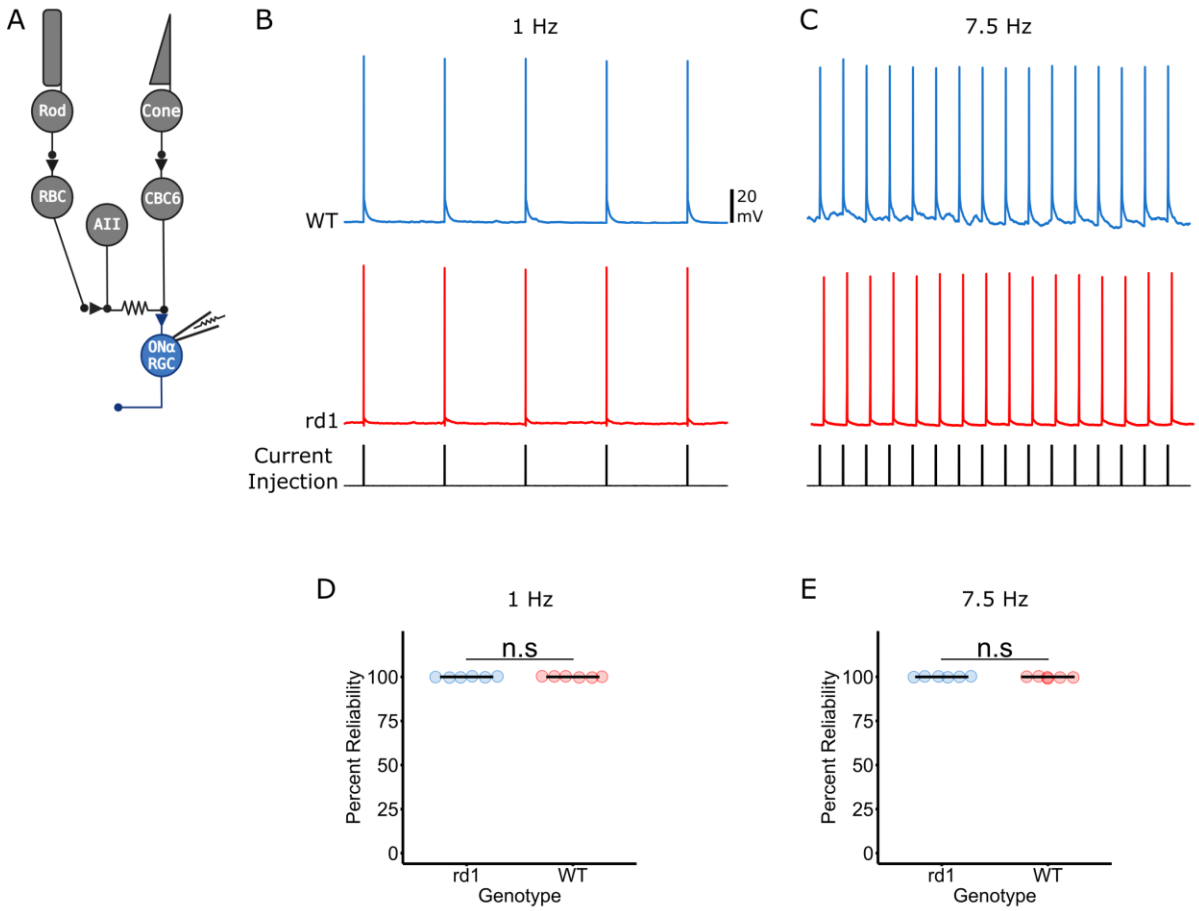

732

733 **Supplemental Figure 6**. **Degeneration does not alter the ability of ON a-RGCs to fire in response to high frequency**
734 **stimulation.** A) Retinal circuit diagrams showing whole-cell patch-clamped ON a-RGCs. B,C) Action potentials from a WT
735 and rd1 ON a-RGC in response to 2.5 ms, 500 pA direct current injection at a frequency of 1 Hz (B) and at 7.5 Hz (C). D,E)
736 There is no difference in ON a-RGCs from WT and rd1 responding to super-threshold current injection at a frequency of
737 1 Hz (p =1) and at 7.5 Hz (p=1). N = 6. All statistical comparisons were made with PWT with FDR correction.